Journal Pre-proof

Laser-based Additive Manufacturing of Bulk Metallic Glasses: Recent Advances and Future Perspectives for Biomedical Applications

Abdul Azeez Abdu Aliyu, Chinnapat Panwisawas, Junji Shinjo, Chedtha Puncreobutr, Roger C. Reed, Kitti Poungsiri, Boonrat Lohwongwatana

Please cite this article as: Abdu Aliyu AA, Panwisawas C, Shinjo J, Puncreobutr C, Reed RC, Poungsiri K, Lohwongwatana B, Laser-based Additive Manufacturing of Bulk Metallic Glasses: Recent Advances and Future Perspectives for Biomedical Applications, *Journal of Materials Research and Technology*, https://doi.org/10.1016/j.jmrt.2023.01.184.

This is a PDF file of an article that has undergone enhancements after acceptance, such as the addition of a cover page and metadata, and formatting for readability, but it is not yet the definitive version of record. This version will undergo additional copyediting, typesetting and review before it is published in its final form, but we are providing this version to give early visibility of the article. Please note that, during the production process, errors may be discovered which could affect the content, and all legal disclaimers that apply to the journal pertain.

Authors Biography

	Dr. Abdul Azeez Abdu Aliyu received his doctoral degree at the Universiti Teknologi PETRONAS, in Malaysia in 2019. He worked as lecturer at Department of Mechanical Engineering, Bayero University Kano, Nigeria since 2014 and currently serving as a postdoctoral fellow in Chulalongkorn University, Thailand. His research interest includes additive manufacturing, synthesis and processing of non-crystalline alloys, biomaterials, synthesis of titania nanotubes for antibacterial drug delivery and processing of biomedical implants.
	Associate Professor Dr. Chinnapat Panwisawas obtained his PhD in Metallurgy and Materials from University of Birmingham, UK (2013). He currently works as Senior Lecturer (Associate Professor) in Materials and Solid Mechanics at Queen Mary University of London (QMUL). Dr Panwisawas has previously joined Rolls-Royce University Technology Centre at University of Birmingham from 2013 to 2018 as Research Fellow. In 2018, he has awarded EPSRC UKRI Innovation Fellowship and became Senior Fellow at Department of Materials University of Oxford. Before joining QMUL in 2022, Dr Panwisawas was Associate Professor in Digital Manufacturing and Associate Director of NISCO UK Research Centre at School of Engineering, University of Leicester.
	Professor Dr. Shinjo Junji received his doctoral degree at the University of Tokyo, Japan. He is currently working as a professor at next Generation Tatara Co-Creation Centre, Shimane University. His research interest simulation and modelling heat flow involved in additive manufacturing processes, thermos-fluid dynamics, and multiphase flow combustion.
	Assistant Professor Dr. Chedtha Puncreobutr holds faculty position in metallurgical and materials engineering at Chulalongkorn University. He has pioneered the metal additive manufacturing and materials modelling for orthopaedics and biomedical applications. He has received numerus awards including Thailand Young Outstanding Metallurgist Award and excellence research awards. He earned his doctoral degree in Materials Engineering from Imperial College London. He also serves as a co-founder of Biomechanics Research Center, Meticuly Co. Ltd.
	Professor Dr. Roger C Reed FREng is currently working as a Professor in the Departments of Materials and Engineering Science, University of Oxford, United kingdom. His research interests include metals processing and modelling. He is serving as an editorial member and reviewer of several international reputed journals. Professor Reed is a Fellow of the Institute of Materials in 2005, a Fellow of ASM International in 2010, and a Fellow of

	Royal Academy of Engineering (FREng) in 2017. He has authored of many research articles/books related to metals processing and modelling.
	Kitti Poungsiri Kitti holds Bachelor degree in Mechanical Engineering, kasetsart University. He worked as researcher at M3D laboratory, Chulalongkorn University and currently serving as Product design Engineer at Meticuly co Ltd.
	Associate Professor Dr. Boonrat Lohwongwatana holds a faculty position in the Metallurgical Engineering Department and Director of Biomedical Engineering Research Center, Chulalongkorn University, Thailand. He earned a Ph.D. in materials science from the California Institute of Technology. He is the recipient of Thailand's Young Technologist Award (2013) from HRH Princess Sirinthorn, and Thailand's Young Metallurgist Award (2015). His is the founder of Biomechanics Research Center, Meticuly Co. Ltd., Thailand. His expertise includes precision manufacturing, 3D printing of titanium, biomechanical designs and standardized testing conforming to ISO 13485 and ASTM standards.

Laser-based Additive Manufacturing of Bulk Metallic Glasses: Recent Advances and Future Perspectives for Biomedical Applications

Abdul Azeez Abdu Aliyu[a], Chinnapat Panwisawas[b], Junji Shinjo[c], Chedtha Puncreobutr[a], Roger C. Reed[d], Kitti Poungsiri[e], Boonrat Lohwongwatana[a,e]*

[a]*M3D Laboratory, Advanced Materials Analysis Research Unit, Department of Metallurgical Engineering, Faculty of Engineering, Chulalongkorn University, Phayathai Road, Wangmai, Pathumwan District, Bangkok 10330, Thailand*

[b]*School of Engineering and Materials Science, Queen Mary University of London, London E1 4NS, United Kingdom*

[c]*Next Generation Tatara Co-Creation Centre (NEXTA), Shimane University, 1060, Nishikawatsu, Matsue 690-8504, Japan*

[d]*Department of Materials, University of Oxford, Parks Road, Oxford, OX1 3PH, UK.*

[e]*Biomechanics Research Center, Meticuly Co. Ltd., Pathumwan, Wang-mai District, Bangkok, Thailand.*

*Corresponding author: Boonrat Lohwongwatana
                Tel.: +66-2-218-6939 (office), Fax: +66-2-218-6942
                e-mail: boonrat@gmail.com

Abstract: Bulk metallic glasses (BMGs) are non-crystalline class of advanced materials and have found potential applications in the biomedical field. Although there are numerous conventional manufacturing approaches for processing BMGs, the most commonly used like copper-mould casting have some limitations. It is not easy to manage and control the critical cooling rate, especially when the fabrication of complex BMG geometries is involved. Other limitations of these techniques include the size constraints, non-flexibility, and the tooling and accessories are costly. The emergence of additive manufacturing (AM) has opened another promising manufacturing route for processing BMGs. AM processes, particularly laser powder-bed fusion (PBF-LB/M) builds parts layer-by-layer and successively fused the powder-melted feedstocks using prescribed computer-controlled laser scanner system, thereby forming a BMGs part upon sufficiently rapid cooling to ensure the glass forming-ability. PBF-LB/M overcomes the limitations of the pre-existing BMGs processing techniques by not only improving the part size, but also produces exceptionally complex structures and patient-specific implants. This review article aims to summarise and discuss the mechanism of BMGs formation through PBF-LB/M for biomedical applications and to highlight the current scientific and technological challenges as well as the future research perspectives towards overcoming the pore-mediated microcracks, partial crystallisation, brittleness and BMG size constraint.

1. Introduction

Owing to the pressing need for low-modulus and low-cost implants, developing new biomaterials with sufficient osteointegration and patient-tailored implant fabrication techniques are highly needed. Metallic biomaterials including stainless steel, Co-Cr, pure Ti and its alloys, pure Zr and its alloys were the most popularly used to fabricate prosthesis, especially for the repair or replacement of diseased bone [1, 2]. The use of other metals such as Mg and Zn alloys were also reported, especially for the synthesis of biodegradable implants [3-9]. Metallic implants are most commonly used for the repair/replacement of hard tissues such as hip and joints, fixation devices, dental implants, cardiovascular stents, screws and bone plates [10, 11]. This is due to their outstanding fatigue and load-bearing capabilities [12]. Among the persistent problems of these crystalline metallic biomaterials is their mechanically incompatible bone elastic modulus (E), which causes stress-shielding effect, thereby resulting in implant loosening/bone resorption and subsequent revision surgery. Other issues include poor wear and corrosion resistance, which lead to adverse reactions, especially when high concentrations of Ni, Al, Cr and Co ions are released into the host tissues after implantation. These problems coupled with low-strength, high cyclic fatigue, insufficient osteointegration and poor biocompatibility limit their long-term performance [13-15]. Thus, development of high quality and much safer biomaterials with acceptable biomechanical properties and relative ease of fabrication is receiving an increasing attention by both academics and industries.

The emergence of non-crystalline alloy referred as amorphous alloys, glassy alloys or metallic glasses (MGs) open-up a new biomedical research area with the over-arching aim to match the bone stiffness. MGs are conventionally produced by suppressing the growth of the crystalline phases and nucleation through rapid cooling of the liquid melts using casting [16, 17]. MGs in the form sheets or ribbon are synthesised by a combination of two or more chemical elements thereby resulting in a glass-like metallic alloys. The existence of MGs can

3

be traced back to 1959 when Klement, et al. [18] discovered Au75Si25 alloy at California Institute of Technology (Caltech), USA. MGs outweighed crystalline metallic biomaterials in terms physical and mechanical behaviours like high toughness and high corrosion resistance. However, MGs are not widely accepted due to their limited size (few microns) which is not sufficient for the industry-scale and clinical applications. The size constraints of the MGs were nearly overcome in early 1990s by bulk metallic glasses (BMGs). BMGs has a much lower cooling rate (10^3 K/s) than the MGs (10^5-10^6) and therefore have a higher critical casting thickness (dimensional constraints imposed by solidification rates necessary to obtain an amorphous microstructure) than the MGs [19]. The first commercial BMG called Vitreloy 1 ($Zr_{42.2}Ti_{13.8}Cu_{12.5}Ni_{10}$-$B_{22.5}$) was developed in 1992 [20]. Since then, several series of BMGs were fabricated with improved sizes (up to centimetres) targeting biomedical and other applications (Figure 1a). In 2004, Xu, et al. [21] presented high glass-forming binary Cu-Zr BMGs at different atomic composition and enhanced mechanical properties. $Cu_{64}Zr_{36}$ was revealed to be the best glass former series among four different BMG series of Cu-Zr observed, whereby the critical casting size of $Cu_{66}Zr_{34}$ was significantly raised from 0.5 mm to 2 mm when the Cu-Zr composition adjusted to $Cu_{64}Zr_{36}$. Another study by Tian, et al. [22] explores on the elastic limit and corresponding stresses of the small binary Cu-Zr MGs through an *in-situ* and quantitative measurement. Compared with bulk specimens, an elevated strain rate and stress values was achieved, as schematically presented in Figure 1b. Other varieties of BMG series with good glass forming ability (GFA) and potential mechanical and biomedical behaviours are presented in Table 1. The non-crystalline nature of BMGs endows them with unique physical and mechanical properties like ultrahigh strength, good corrosion and wear resistance, excellent elastic behaviour and near-to-bone E when compared with the crystalline alloy counterparts [23-36]. The thermodynamically non-equilibrium nature of BMGs resulted in constant changes of their local structures during structural relaxation and mechanical

4

deformation. This provide an in-depth understanding of their structural origin for various mechanical behaviours resulted from structural heterogeneities [37, 38]. The behaviours of various BMGs, BMG composite and other engineering materials like fracture toughness, strength and density were summarised and compared through Ashby maps in Figure 2.
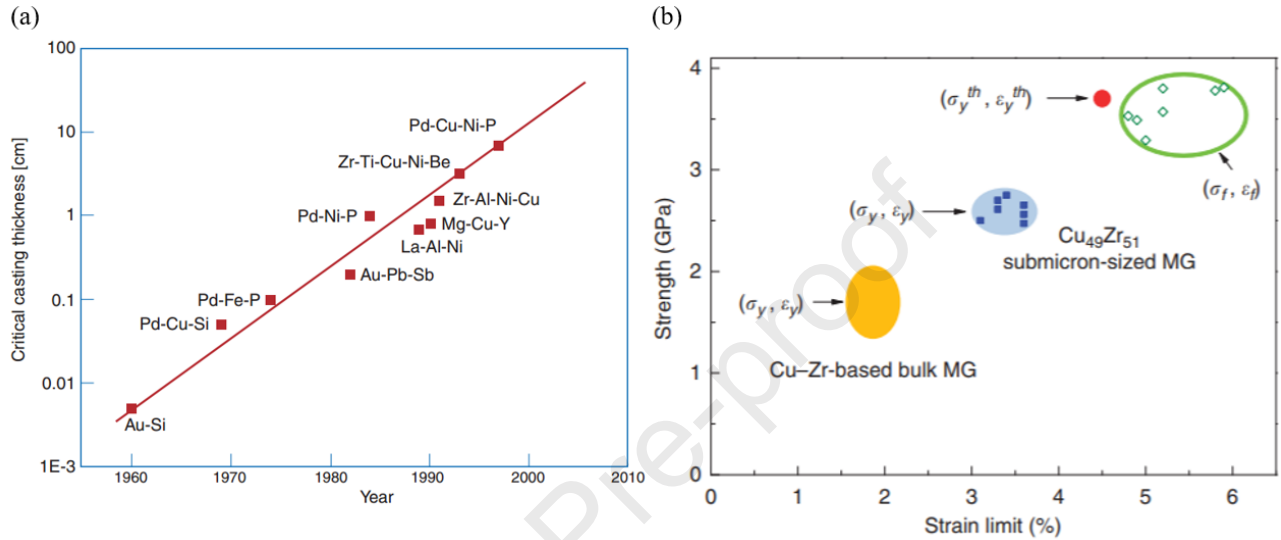

Figure 1: (a)Various varieties of BMGs indicating year of its discovery versus the critical casting size for the amorphous formation (b) Comparison of the small binary and bulk Cu-Zr BMG elastic strain and the corresponding stresses. The strain rate and stresses of the bulk Cu-Zr MGs is indicated by the yellow solid ellipse while the yield strain and strength are of the small MGs is donated by the green square solid. The measured fracture strength and the fracture strain are presented by the blue open diamond [22, 39]
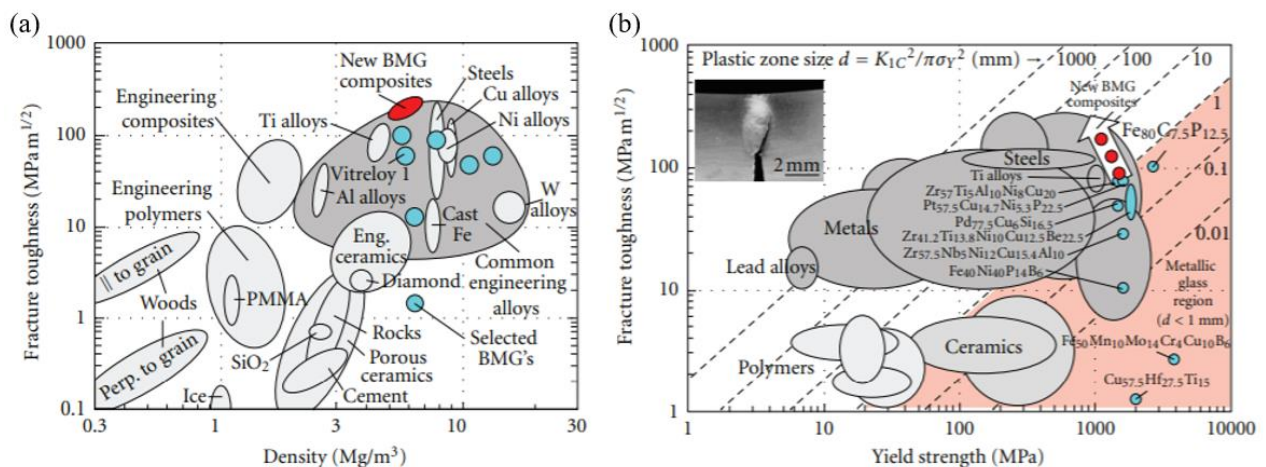
Figure 2: Ashby Maps showing the relationships between some selected BMGs, BMG composites and other various engineering materials with fracture toughness and (a) density (b) yield strength [40]

Currently, BMGs are conventionally processed through various metallurgical processing routes like powder metallurgy [41-46], rapid cooling of liquid melts [40, 47-49], melt spinning [50, 51], magnetron sputtering [52-54], pulsed laser quenching [55, 56], liquid splat quenching [57], electro-discharge machining/coating [58-64], and thermoplastic forming [65, 66]. It has to be noted that, melt spinning and thermoplastic forming are currently well-established BMG processing techniques. Despite great improvement in achieving the BMGs size, to date, these techniques could not produce sufficient size for the industrial and biomedical use. Other limitations of these conventional methods are their inability to easily fabricate complex and patient-specific implants without compromising the initial properties of the BMG. Additionally, the cost of the BMG processed through these techniques is high.

Additive manufacturing (AM), also known as 3D printing, is a novel technological innovation, which involved building a bulk part using computer-aided design (CAD) model through layer by layer deposition of the metal melts [67, 68]. Laser-based additive manufacturing (LAM) are AM processes, which utilizes laser source as the heat source and laser beam to rapidly melt metal powder. LAM is used in various industries like biomedical [69-73], aerospace [74, 75] and tool-making [76]. LAM gains some advantages over the conventional machining and powder metallurgy techniques. These include formation of fine grain size and enhanced mechanical behaviours due to its high energy density and rapid cooling rate [77], ease of moulding difficult to machine materials due to high melt pool temperature [78], processing of functionally graded material due to its ability to change the chemical composition of the input material [79] and fabrication of highly complex geometries [78]. LAM is mainly classified into laser powder-bed fusion (PBF-LB/M) AM and laser-based direct

energy deposition (L-DED) AM, also called laser metal deposition (LMD), laser cladding (LC) or laser engineered net shaping (LENS) [77, 80-83]. Figure 3 shows various classifications and the phrases of laser-based AM.
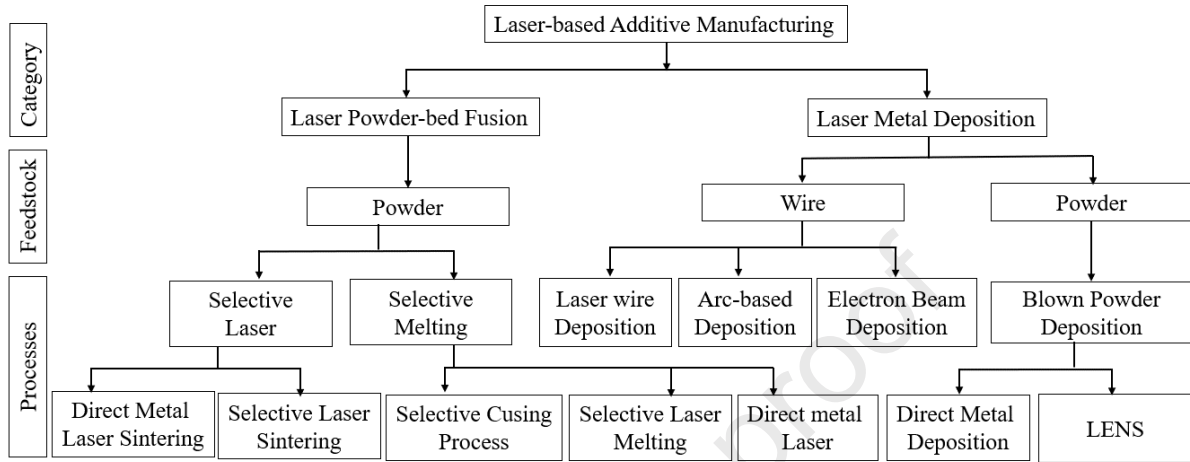

Figure 3: Various classifications and phases of laser-based additive manufacturing

Table 1 Various biomedical BMGs synthesized through several routes indicating their achieved sizes, mechanical and biomedical behaviours

BMG Series /Composition	Diameter (mm)	Synthesis Method	Mechanical/biomedical Behaviours	Ref.
Ti-based BMGs				
TiCuHfSi	3	Copper-mould casting	• Fracture toughness 1685 MPa • Young Modulus 95 GPa • Good corrosion resistance	[84]
Ti–Cu–Zr–Fe–Sn–Si–Ag	7	Copper-mould casting	• High specific strength • Young Modulus 100 GPa • Good corrosion resistance	[85]
Ti–Zr–Cu–Fe–Sn–Si	3	Copper-mould casting	• Yield strength 1750-1800 GPa • Hardness 606-613 Hv • Young Modulus 100 GPa • High corrosion resistance	[86]
Ti42Zr40Si15Ta3	-	Powder metallurgy	• Yield strength 140 -730 GPa • Young Modulus 8-53 GPa • Good osteointegration	[87]
Ti-Cu-Zr-Fe-Sn-Si-Ag-Pd	4-5	-	• Hardness 591-610 Hv • Compressive strength 2074 -2340 GPa • Young Modulus 100 GPa • Good Biocompatibility	[88]
Zr-based BMGs				
Zr61Cu17.5Ni10Al7.5Si4	-	Melt spinning	• Hardness 510 Hv • Compressive strength 1800 MPa • Good Corrosion resistance	[89]
$Zr_{61}Al_{8.9}Fe_{10.2}Cu_{10.2}Ag_{9.7}$	16	Copper-mould casting/Arc melting	• High specific strength 2.3×10^5 Nm/kg • Young Modulus 80 GPa • Good adhesion	[90]

$Zr_{59.3}Cu_{28.8}Nb_{1.5}Al_{10.4}$	1.5	Additive Manufacturing	▪	Fracture toughness 24−29 MPa√m	[91]
$Zr_{0.5}Ti_{0.02}Cu_{0.38}Al_{0.1}$	5	Copper-mould casting	▪ ▪ ▪ ▪	Yield strength 1750-1800 GPa Hardness 606-613 Hv Young Modulus 82-89 GPa Good Biocompatibility	[92]
$Zr_{52.1}Ti_5Cu_{17.9}Ni_{14.6}Al_{10}Y_{0.4}$	1-5	High pressure die-casting	-		[93]
Fe-based BMGs					
$Fe_{41}Co_7Cr_{15}Mo_{14}C_{15}B_6Y_2$	3	Copper-mould casting	▪ ▪ ▪	Hardness 1122 Hv Compressive strength 4000 MPa Good Corrosion resistance	[94]
Fe55Cr8Mo14C15B6Er2	>4	Copper-mould casting	▪ ▪ ▪	Hardness 1122 Hv Young Modulus 209 GPa Fracture strength 4.4 GPa	[95]
Fe–Cr–Mo–(Y,Ln)–C–B	12	Copper-mould casting	▪ ▪	Micro Hardness 13 GPa Young Modulus 180-200 GPa	[96]
FeCoCrMoCBY	16	Copper-mould casting	▪ ▪	Hardness 1253 Hv Fracture strength 3.5 GPa	[97]
Ca-based BMGs					
$Ca_{65}Mg_{15}Zn_{20}$	15	Copper-mould casting	-		[98]
$Ca_{60}Mg_{20}Ag_{20}$ Ca60Mg20Ag10Cu10	4 7	Copper-mould casting	- -		[99]
$Ca_{60}Mg_{20}Zn_{20}$	Plate	High-pressure die casting	▪ ▪	Excellent corrosion resistance Biodegradable and Bioresorbable	[100]
Zn-based BMGs					
Zn–Mg–Ca–Yb	2	Copper-mould casting	▪ ▪ ▪	Low E High corrosion resistance Compressive strength 663	[101]
Zn38Ca32Mg12Yb18	2	Copper-mould casting	▪ ▪	Young Modulus 36.6 Compressive strength 640	[102]

PBF-LB/M AM techniques were recently utilised in fabricating various geometries and types of implants including jaw, cranial or maxillofacial, ribs and sternum, pelvic, hip cup, hand, toes and knee [103], as depicted in Figure 4. In recent years, the use of PBF-LB/M AM techniques to processed BMGs is widely studied [104-107]. It has to mention that, plasma spray or cold spray initially developed to coat metallic substrates, is another powder-based AM approach recently utilized and shows high potential in producing large-sized BMGs or BMG composites with turnable properties like ease to impart porosities or composite microstructures [108]. Plasma spray AMed BMG parts have less thermal stresses and the process requires less heat input, thus, it produces BMG parts with high amorphous content (> 95 %) and crack-free surface [109, 110]. It has high efficiency and do not require any protective (atmospheric) chamber during the process [111, 112]. The working principle of plasma spray AM involved

8

preheating of metallic glass powder at very short duration (0.5 ms), then, the semi-molten particles are deposited at supersonic velocity to form BMG parts or BMG composites. However, this method is not yet applied in producing wide range of BMG alloys. Current reports are specifically on processing of Fe-based BMGs. Fused filament fabrication (FFF), is another AM technique recently employed to fabricate highly amorphous BMGs using MG rods as feedstocks [113]. However, this method is more explored in the processing of thermoplastics and seldom use in fabricating BMGs. Therefore, this paper will focus on the BMGs processed through PBF-LB/M AM approaches. PBF-LB/M AM involved a repetitive layer-by-layer melts fusion and solidification at a very high cooling rate ($10^4 – 10^7$ K/s). This, in combination with other factors like the alloying elemental composition and the fabrication method type, resulted in a fully or partially amorphous structure. The amorphous phase formation depends strongly on the thermal stability, GFA of the alloying elements and the process parameter settings [114, 115].
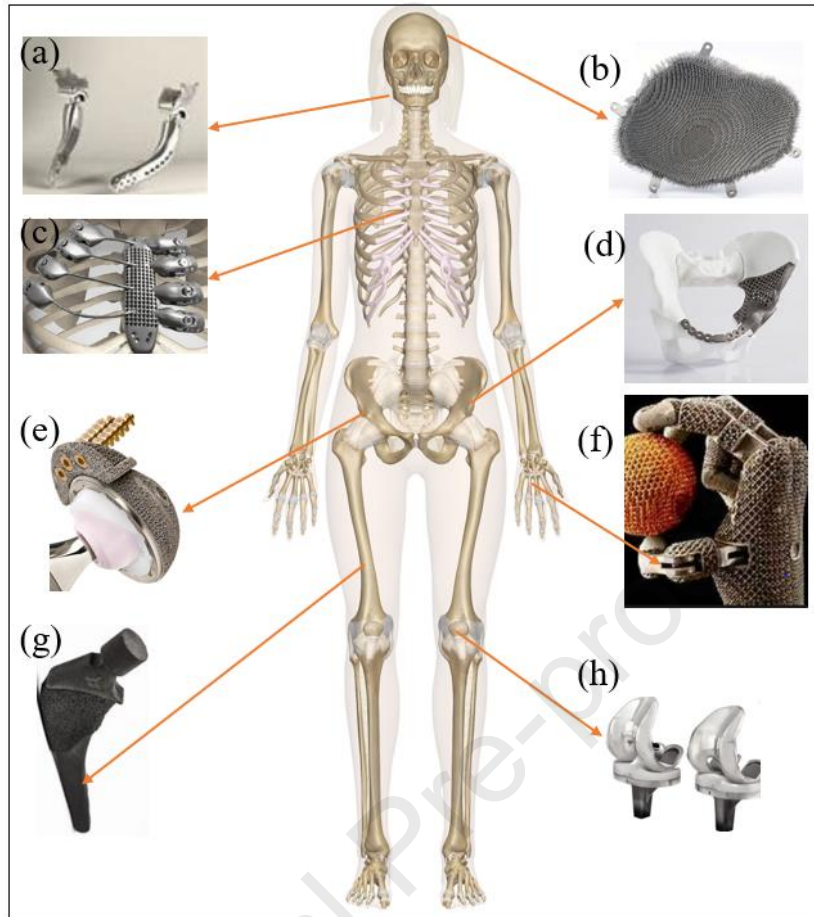
Figure 4: Various implants processed through PBF-LB/M AM process (a) jaw implant [116] (b) cranial implant [117] (c) ribs and sternum [118] (d) pelvic implant [119] (e) hip cup implant [120] (f) hand and toes implants [121] (g) hip implant [122] (h) knee implant [123]

The benefits of PBF-LB/M AM techniques over the conventional BMG fabrication methods is not only in fabricating BMGs larger than the critical casting size [124-126], but also in fabricating a complex geometries and patient-specific geometries [127-129]. Moreover, PBF-LB/M AM techniques do not require tooling pre-production and part-specific tooling costs. Thus, it is cost-effective and foreseen as the potential BMGs fabrication methods for the industries, especially the fabrication of biomedical parts [127, 130, 131]. While maintaining the products quality, PBF-LB/M AM is a good candidate for mass production of medical devices [132]. PBF-LB/M is widely employed in processing BMGs over other LAM processes. This might relate to its ability to produce high resolution features, sufficient energy to melt MG

powders and flexibility in MG powders alloy combination. The major challenge in the fabrication BMGs through PBF-LB/M is the cyclic thermal impact during the process, which results in relaxation phenomena. Recently, the mechanisms of PBF-LB/M AM operation and their potentials for producing complex and customise BMG implants has been widely studied. Aside from a strong potential of 3D printed BMGs in the medical field for the fabrication of customized and patient specific biomedical implants [133], they are utilized in the aerospace industry, especially for the fabrication of gears to operate under cryogenic conditions [134-136] as well as watches and jewellery industry [137, 138].

Although, recently, Zhang, et al. [139] published a comprehensive review on 3D printing of BMGs. This review focuses mainly on PBF-LB/M techniques and processing of BMGs, specifically for biomedical applications. It also summarised the reports of various studies on the processing of BMGs through PBF-LB/M AM techniques. Furthermore, the current challenges of PBF-LB/M AM techniques in fabricating the BMG parts are outlined and the future research trends is proposed. Figure 5 shows a schematic 3D illustration of the PBF-LB/M process [140].
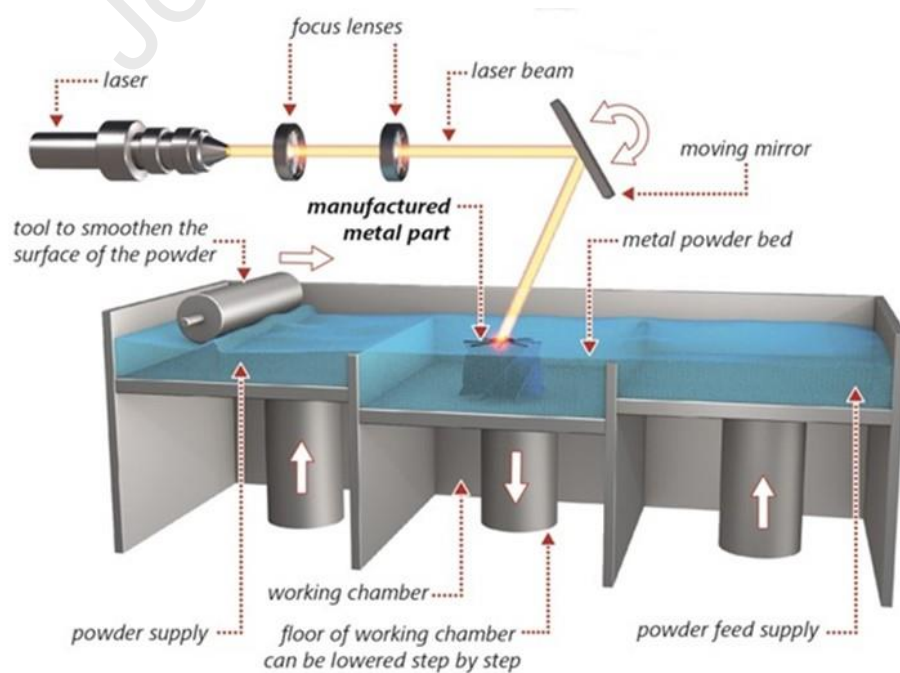

11

Figure 5: 3D illustration of PBFPBF-LB/M process for part layers built on the XY surface [141]

2. Bulk metallic glasses

BMGs are non-crystalline or amorphous alloys, which are formed through the combination of three or more chemical elements to achieve certain properties for a specific application [142]. The major advantage and unique features of BMGs over crystalline alloys is that they do not possess grain boundaries or crystal dislocation defects. Thus, they have exceptional combination of physical, biomechanical and biomedical characteristics with a very high strength, an elastic limit near that of the theoretical value and good biocompatibility [95, 143, 144]. This makes them as good candidate for the development of biomedical implants, especially for the repair/replacement of load bearing tissues [145-147]. For instance, a common Zr-based BMG with an elastic limit of 2 % can yield up to 2,000 MPa while the Ti-based implant material with an elastic limit of 0.7 % can only yield less than 800 MPa [148]. Insufficient size, high brittleness and inadequate BMG parts fabrication techniques are the major downside of the BMGs to be used in the orthopaedics and medical industries.

2.1 Formation of biomedical BMGs

Conventionally, metallic alloys are formed by selecting the main chemical element based on the required primary mechanical and chemical property. Then, the secondary properties are achieved by addition of alloying elements, thereby forming a multicomponent system of alloys. For instance, an alloy of bio-metallic or biomedical BMGs is formulated by combining biocompatible elements such as Zr, Ti, Fe, Ca, Mg or Zn with other non-toxic chemical elements that have a specific desirable property. This enhanced the MGs structural disorder by forming higher degree of element multiplicity and hence, improve the GFA of the alloy [149]. Subsequently, the alloy is converted to an amorphous or bio-metallic glass structure through

12

heating and subsequent rapid cooling, sufficient to avoid crystallisation (Figure 6). Thus, the structural amorphous features of the material coupled with the flexible elemental compositions produce different forms of BMGs for specific functions like biomaterials [150-152], catalysis [153], antibiosis [154], magnetic [155-157] and structural materials [30, 143]. The essential consideration during the formation of biomedical BMGs largely depends on the non-toxicity and biocompatibility, GFA, as well as physical and mechanical behaviour of the alloying elements.
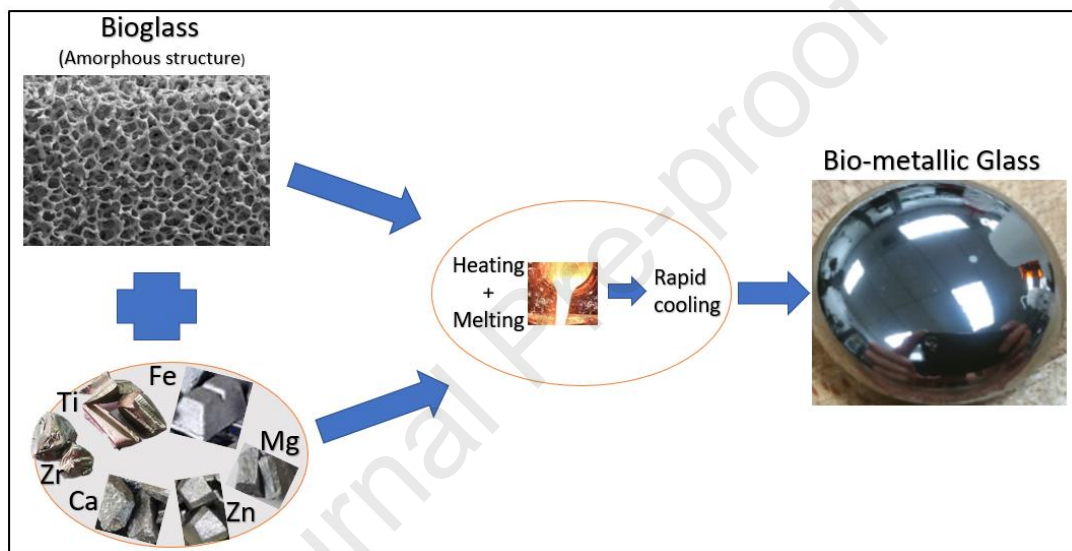

Figure 6: Formation of biomedical BMGs from bioglass and biometallic alloys

2.2 Non-toxic and biocompatible alloying elements

Toxicity refers to the behaviour of biomaterial to release a harmful substance to the host body after implantation, which may affect the cells, organs or the whole body. Biocompatibility is the ability of the biomaterial to perform for long-term in the living body without eliciting any harmful effect to the human tissues [158]. Generally, a good biomaterial should be non-toxic and possess excellent biocompatibility. Most metallic elements are present or consumed in the human body either in high or very small quantity. However, there is no synthetic metallic elements that are completely bioinert or non-toxic. This means that, the metallic elements might

13

become toxic if used beyond the body requirement. Developing biomedical alloys thus requires the proportionate use of elements which are practically bioinert or the elements which exist essentially in macro or trace concentration in the human body [159]. Almost 96 % of the body weight is formed by water and protein, which basically contained oxygen (O_2), carbon (C), hydrogen (H_2) and nitrogen (N_2), while the remaining 4 % are mainly in the form of minerals (Ca, Mg, P) in the bone, electrolytes (Na, K, Cl) in the blood and extracellular fluids as well as sulfur (S) in the body. Other trace elements in the body, which might be added to the biomedical alloy in an extremely low quantity include Fe, Cu, Mn, iodine, Zn, Se, Co and Cr [160]. Some metallic elements such as Zr and Ti are proven virtually inert and non-toxic to the human body [161]. These elements are mainly used in high quantity for developing a biomedical BMGs, due to their high strength, resistance to corrosion and wear and excellent biocompatibility [162].

2.3 Concept of glass-forming and forming abilities

The most common method of fabricating BMGs is through a rapid quenching of the molten metal alloy at a very slow cooling rate of 10^{-2} to 10^6 K/s [163, 164]. Thus, the detectable crystallisation and nucleation are avoided and hence the glassy structure is achieved, as shown in the time-temperature transformation (TTT) diagram (Figure 7a). GFA refers to the maximum amorphous thickness or diameter of a specimen fabricated through rapid cooling of the metal melts [165]. Quantitatively, GFA is an inverse of the critical cooling rate. That is to say, the lower the cooling rate required to bypass crystallisation, the more the fully amorphous structure is produced [166, 167] (Figure 7b). Since the emergence of BMGs, GFA of the alloying elements or the alloy systems to achieve large BMG size remain the key concern. There are three main factors contributing to the GFA, these include (i) multicomponent alloy consisting of at least three chemical elements, with (ii) more than 12 % different atomic size ratio and (iii) high negative enthalpy of mixing [168, 169]. Generally, an alloy with composition near the

14

eutectic points are considered good glass formers and all glass formers are characterised by relatively low melting temperature, highly reduced glass temperature and strong interactions between the atoms constituents [170]. Some researches focusing on the alloying elements promoting or inhibiting the glass formation of the BMGs were reported. Zai, et al. [171] investigated the role of Ga addition on the GFA of Mg-Zn-Ca BMG and found that, the added Ga enhanced the GFA of the Mg-Zn-Ca BMG by increasing its critical diameter from 3.5 to 5.0 mm. On the other hand, Ag was found to decrease the BMG sensitivity to temperature thereby reducing its GFA. Thus, substituting Ag for Fe from the $Zr_{60}Cu_{25}Al_{10}Fe_{5-x}Ag_x$ BMG significantly rise its GFA [172]. The highest increase in GFA was observed when Ni and Pd were added to $Zr_{48}Cu_{36}Al_8Ag_8$ alloy while substitution of Cu or Zr for Au or Hf, respectively, slightly lower the GFA. Moreover, addition of Ti, Ni and Fe greatly reduce the GFA of the alloy [172]. Another study by Park, et al. [173] revealed that, substituting Ni and Ag for Cu in the $Cu_{60}Zr_{30}Ti_{10}$ alloy improved the GFA of the $Cu_{40}Ni_5Ag_{15}Zr_{30}Ti_{10}$ BMG. Partial substitution of Ni for Pd increased the GFA of Zr-Al-Ni thereby increasing its critical diameter from 3 to 5mm [174]. Similarly, partial substitution of Hf for Cu enlarges the supercool temperature of the $Zr_{55}Ti_3Cu_{32}Al_{10}$ BMGs and hence, greatly enhanced its GFA and increased the diameter from 4 to 8 mm [175]. Recently, various multicomponent systems of toxic element-free and biomedical BMGs with high GFA were reported. These include $Ti_{40}Zr_{10}Cu_{36}Pd_{14}$, and $Zr_{48}Cu_{36}Al_8Ag_8$ [151], $Zr_{56.25}Al_{18.75}Co_{18.75}Cu_{6.25}$ [176], $Ti_{40}Zr_{35}Cu_{17}S_8$ [177], $Ti_{47}Cu_{38}Zr_{7.5}Fe_{2.5}Sn_2Si_1Ag_2$ [178], $Ti_{47-x}Cu_{40}Zr_{7.5}Fe_{2.5}Sn_2Si_1Sc_x$ [179], $Ti_{45}Zr_{10}Cu_{31}Pd_{10}Sn_4$ [145] etc.
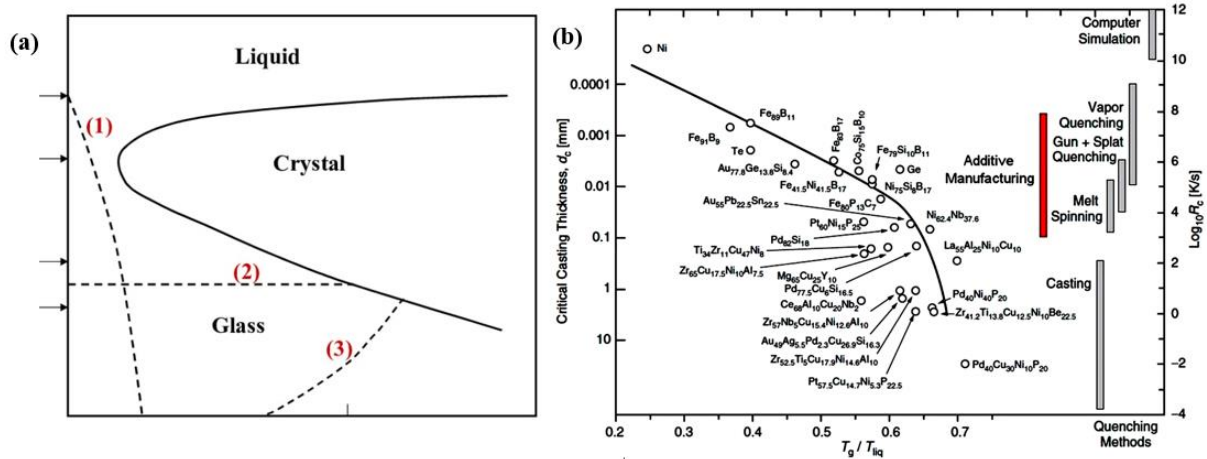
Figure 7: Schematic illustration (a) TTT diagram showing growth of crystal in an under melt phase (1), glass formation due to rapid cooling (2), crystallisation at time t_x due to glass isothermal heat treatment and crystallisation Tx due slowly glass heating (b) Relationship between reduced transition temperature (T_g/T_m), critical cooling rate (R_c) and critical casting thickness for the MGs and BMGs [180-182]

2.4 Physical and mechanical behaviour of the alloying elements

Physical properties of metals such as density, thermal conductivity, specific heat, melting point, corrosion and thermal expansion are the most important criteria used in selecting the metallic alloying elements. Specific strength (strength-to-weight ratio) and specific stiffness (stiffness-to-weight) are density dependant. To fully understand the mechanism of glass formation, amorphous solid critical heating rate and assessing the critical cooling rate for the amorphous formation, thermophysical properties play a very vital role [183, 184]. The rate of resistance to corrosion of BMGs highly depends on the corrosion deterioration or wear rate of the individual chemical elements in the host body. Therefore, careful selection of the alloying metals is the common way of preventing corrosion of an alloy in the working environment [185]. To achieve a specific function of the BMGs, mechanical properties of the alloying elements such as ductility, strength, toughness, modulus of elasticity and strain hardening must be considered. For instance, addition of Ni to Fe-B-Si-P-Nb BMGs greatly enhances its

ductility [186]. The GFA and mechanical properties of Ti–Zr–Be were significantly increased by the addition of Fe to the alloy [187].

3. Laser powder-bed fusion of BMGs

The concept of PBF-LB, specifically selective laser melting (SLM), as indicated by Yap, et al. [188], was first introduced by M. Fockele and D. Schwarze of F & S Stereolithographietechnik GmbH, as well as byW. Meiners, K. Wissenbach, and G. Andres of Fraunhofer ILT. It has to be noted that, the terms SLM, LPBF and PBF-LB/M are synonyms and are terminology of AM processes defined in ISO/ASTM 52900 [189]. SLM is the most versatile form of AM and PBF-LB/M processes, and are promising techniques for producing various 3D metallic, polymers and ceramic components [190-193]. The working principle of SLM involved selective melting of metallic powder on a build platform using a laser beam. The 3D data obtained from the CAD model is converted to 3D components through layer-by-layer deposition [194]. Like conventional techniques, SLM produces a bulk part from a combination of different elemental powders to achieve a desired property. The conventional BMG fabrication techniques has constraints in fabricating large BMG components [195] due to extremely fast cooling rate. SLM overcomes this limitation by producing bigger parts than the critical casting size [196-198]. Other advantages of the SLM process over pre-existing BMG fabrication methods include fabrication of geometrically complex parts and that wide range of BMGs can be produced with not only high GFA materials, but also materials with weak GFA or low critical casting thickness. When SLM process parameters such as laser parameters, are properly optimised, it can produce an alloy with strong, ductile and low E due to the capability of SLM in fabricating fully dense part with tailored microstructure after solidification [199]. The application of SLM in the fabrication of amorphous silicate glasses and metallic glasses has recently been reported [200-203].

3.1 Cooling and solidification in PBF-LB/M

The mechanism of energy transfer during PBF-LB/M follows the inverse bremsstrahlung absorption mechanism or the collision absorption of the laser light [204]. The high energy (10^5-10^7 W/cm^2) transferred is enough to melt and sometimes evaporate an alloy of metallic powder within a very short time (10^{-3}-10^{-2} s) [205, 206]. Thus, a small pool of the molten alloy is formed and quickly solidifies at an extremely fast cooling of 10^3 - 10^8 K/s, when an incomplete melting or evaporation is successfully averted [207, 208]. The cooling rates of an alloy might vary at different PBF-LB/M processing parameters while the input energy maintained constant [206]. The cooling rates in PBF-LB/M processes are mostly higher when compared to that of conventional casting, especially for obtaining amorphous alloys. During PBF-LB/M of BMGs, in every scan, a very small volume of metal powder is melted and quenched rapidly at extremely high cooling rate ($>10^4$ K/s) far higher than that of conventional glass formation (10 - 10^4 K/s) [209], thereby resulting in a fully amorphous structure. The subsequent rapid solidification of the metal melts produces various microstructure of the PBF-LB/M processed parts. Thus, the physical, mechanical and chemical properties of such alloys can be tailored to achieve a specific function. The metal-laser interaction coupled with melting and subsequent solidification resulted to heat affected zone (HAZ), a zone, where partial crystallization occurred. High oxygen content enlarges the HAZ in the BMG matrix and hence, more crystallization [210]. Despite the rapid cooling involved in the PBF-LB/M processes, a wide range of cooling rates is normally observed. Therefore, BMG requires proper thermal stability to maintain the thermal cycling [211]. In a microstructural study of Al-Cu alloy to determine the cooling rate of an individual melt track during PBF-LB/M, it was found that the cooling rate decrease towards the boundary from the central part of the melt track [212]. In another study using different metallic alloys, the cooling rates show similar trends, whereby it reduces from the centre of the molten metal to its boundaries [207, 213].

18

3.2 Thermal history

The layer-by-layer deposition mechanism of PBF-LB/M bestowed its unique thermal history, which resulted in a particular solidification behaviour [188, 214]. Therefore, monitoring the special temperature during PBF-LB/M is quite challenging. The PBF-LB/M process is highly dynamic, whereby the material is molten and repeatedly solidified during the process. This necessitates the need for an in-situ temperature monitoring of PBF-LB/M processes. Over the past years, various studies on AM processes monitoring and control were reported and revealed that, thermocouples, pyrometers and displacement sensors were the most used devices [78, 215-219]. Most of the published articles concerned on the melt-pool temperature monitoring during the PBF-LB/M processes. Thermocouples and spectrum of embedded optical sensors were employed by Kousiatza and Karalekas [220] and developed an in-situ real-time monitoring system to monitor the temperature and strain profiles of the PBF-LB/M processes. The findings confirmed an accurate system for the measurement of the residual strains and temperature variations. Another study by Rao, et al. [221] who developed a sensor-based process monitoring system using thermocouples, infrared temperature sensor and accelerometers to identify and detect the failure modes in PBF-LB/M processes, through evidence theory and Bayesian Dirichlet mixture [222]. The system was found to have an accuracy of about 85 %. Vallabh and Zhao [223] used single camera two wavelength imaging pyrometer to monitor and measure the melt pool temperature during PBF-LB/M process. The system was confirmed to accurately monitor the molten pool temperature as well as its variations at high framerates for 50 layers.

To deeply understand the thermal history and temperature evolution during PBF-LB/M, the thermal field in a glass-forming alloys is simulated using finite element method (FEM) by several researchers [224-227]. In a study to calculate the historical temperature evolution and its distribution, the melt pool of the Zr-based BMG was found to solidify at a high rate of about

10^4 K/s and monolithic glasses were observed [228]. However, it is found that the temperature in the HAZ exceeded that of crystallisation. At this instance, crystals may precipitate or not in the HAZ, depending on the duration of such elevated temperature. Based on the simulation, the duration at which such high temperature to remain in crystallisation temperature can be almost 5 mins and hence, only nanocrystals are observed [229]. Thermal history can affect the mechanical properties of the BMGs due to the possible formation of heterogeneities within the alloy [230]. A model of BMG, which predicts the thermal history during PBF-LB/M at every simulation stage is reported by Lindwall, et al. [231]. Finite element BMG simulation through PBF-LB/M AM showing the 3D contour plot temperature field and phase model prediction of the crystalline fraction is depicted in Figure 8.
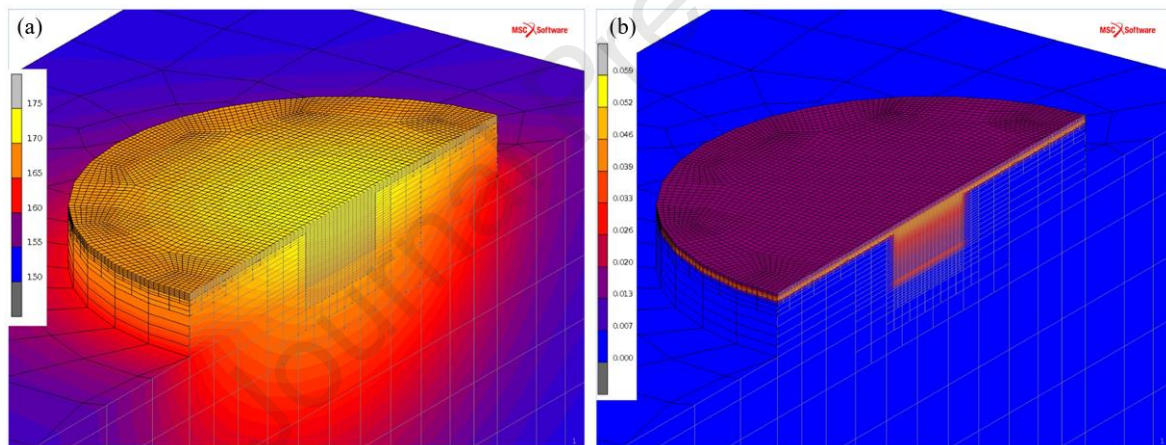

Figure 8: Finite element BMG simulation through PBF-LB/M AM showing (a) 3D contour plot temperature field at one second after deposition of the 50th layer (b) phase model prediction of the crystalline fraction [231]

3.3 The thermal stresses and temperature gradients

In a layer-based manufacturing processes like PBF-LB/M, the material deposition involved temperature gradients between the adjacent layers resulted in thermal stresses [232, 233]. A steep temperature gradient is developed as a result of rapid cooling of the top layer and subsequent slow heat conduction by the layer beneath it. When the top layer is heated, it will

attempt to expand, but the neighbouring materials will inhibit the expansion, thereby resulting in compressive strains (elastic and plastic) (Figure 9a). This phenomenon will continue until the yield strength of the material is reached. Thus, rapid solidification, due extremely fast cooling coupled with expansion constraints from the adjacent solidified layers, developed tensile stress at the bottom layers (Figure 9b). Normally, thermal stresses resulted in inaccuracies and distortions, which may lead to mechanical failure of the BMG part by cracking. For instance, when the next powder is scanned or heated, the thermal stresses are partially relieved and accumulated in the successive layers. This induces the crack formation (Figure 9c), which in most cases propagate from the pores, especially when low laser energy (LE), also referred to as energy density is used in processing the BMG part [234, 235]. Remelting and chessboard scanning strategy effectively eliminates the micro-cracks of the PBF-LB/M fabricated Fe-based BMG [236]. Another study by Li, et al. [237] confirmed that, remelting of the BMG layer by employing high power initial scan and re-melt using low power relieved the residual stresses, and hence crack is inhibited. The nature of the thermal stresses formed can be controlled by optimizing various PBF-LB/M process parameters such as scanning strategy, LE, layer thickness and laser power. Depending on the scan strategy and part geometry used, time-varying processing temperatures can induce other types of internal stresses within the PBF-LB/M processed part. Normally, vectors parallel to each other are used to scan the cross-sections of the part during PBF-LB/M process. A short scan vector length occurs when the area is small, leading to a high temperature due to little cool down time [238]. However, for a large area, the successive tracks require more time to cool the entire area, because the laser beam travel much longer and hence, resulted in a low temperature. This reduces the density of the material due to worse wettings conditions.
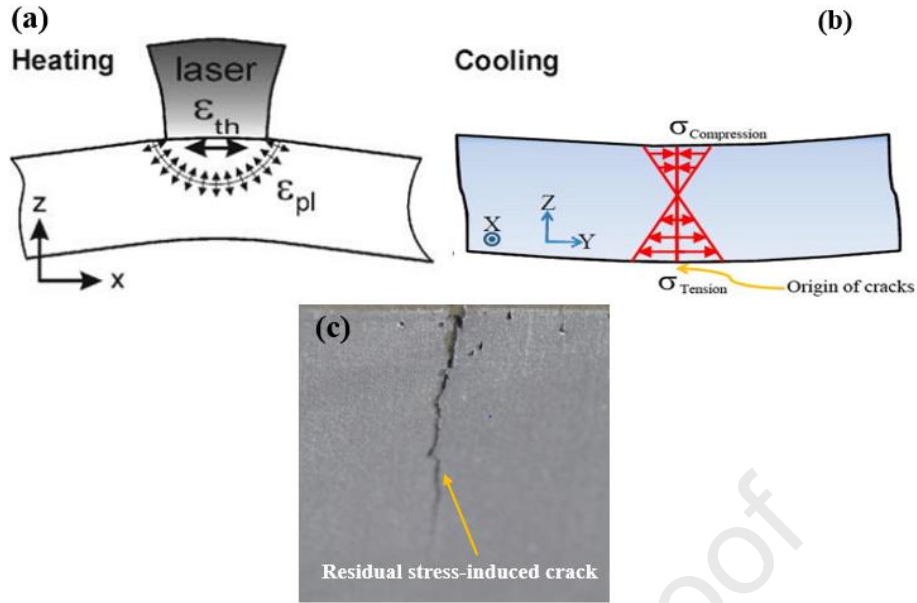
Figure 9: Schematic illustration of the thermal stress behaviour (a) mechanism of temperature gradients (b) position of cracks in PBF-LB/M processed part (c) microstructure of the 3D printed part indicating residual stress-induced crack [238, 239]

3.4 PBF-LB/M process parameters

Processing of BMGs through PBF-LB/M is influenced by several parameters. These include scan speed (v), laser power (P), scan spacing (s), layer thickness (t), and scanning pattern (Sp) [188]. These parameters affect the input energy, which in turn strongly affects the microstructure and the heat distribution of the processed BMG. The input energy is determined by the LE, which is related by P, v, s, t in equation 1 [240]:

$$LE = \frac{P\ (W)}{v\ (mm/s)\ x\ s\ (mm)\ x\ t\ (mm)} \tag{1}$$

The LE-value strongly influence the amorphous nature and hence, the properties of the final BMG components. Thus, the quality of the biomedical BMG component is highly affected. Therefore, proper selection and optimisation of the parameters for processing BMG components through PBF-LB/M is expected to solve these problems [241, 242]. Although scanning pattern (scanning strategy) is taken care in the PBF-LB/M parameter optimization by

22

some authors [243, 244], other important factors like laser diameter, laser corners and surface offsets and the gas flow directions are not covered, which might directly or indirectly affect the microstructure of BMG parts [245].

3.4.1 Influence of PBF-LB/M parameters on pores formation

The bone-matched controllable or designed porosities produced through PBF-LB/M are beneficial to biomedical implants. Generally, porous implants have lower E than the fully dense alloy with the same composition. An implant with low E close to that of human bone have less stress-shielding effect and enhanced long-term *in-vivo* life span [246]. Additionally, porous implants promote biological tissue ingrowth and adhesion into the porous structure, thereby enhancing the *in-vivo* stability of the implant [247]. PBF-LB/M allows controlled pores design and fabrication of the implant to match natural bone structure. On the other hand, some unintended or undesigned pores might be formed within the PBF-LB/M BMG part, especially if the parameters are not properly controlled or optimized. Thus, fatigue cracks are initiated from these pores (pore-mediated microcracks), thereby degrading the mechanical properties and long-term performance of the implants [248, 249]. In PBF-LB/M, the LE plays a greater role in the pore formation. This implies that the lower the power, the lower the LE and hence, less porosities are formed. Lower or insufficient energy produces highly amorphous, but there is high tendency of incomplete powder melting, which might result in the formation of highly porous BMG part. When the LE-value is too high, melts instability (balling) occurred [194], and the melts vaporizes [250]. Hence, the BMG parts becomes less dense. To reduce balling, modest LE-value is used, but resulted in an interlayer and large open pores, due to inadequate inter-layers filling and partial re-melting. Xing, et al. [251] applied LE with value higher than 20.83 J/mm^3 and found no interlayer or open pores, except small size metallurgical pores, which occurred due to escaping gas evaporation. Another PBF-LB/M parameter that plays vital role in the pore formation is the scanning strategy. Unmodified scanning strategy can

significantly affect the relative density [252], and pores distribution [253]. Incomplete powder melting is also observed when there is an inconsistent scan speed and too thick layer thickness, which resulted in the pore formation [254, 255]. Laser power also plays a key role in the pore formation, low power resulted in the formation of large and irregular porosities, due to incomplete melting of the powder particles. The pores decreases by increasing the power due to more melting of the metal powder [242, 256]. Qiu, et al. [257] studied the role of melt flow on the surface structure and porosity during PBF-LB/M of Ti-based implant and found that, high laser speed and power increases the pore formation. Additionally, unstable flow and powder thickness were reported to have strong influence on the pore formation. A similar study by Read, et al. [258] revealed that, the laser power, scan speed and the interaction of scan speed and spacing have a strong influence on the PBF-LB/M processed part. The fabricated specimen was found to have superior strength and elongation behaviour compared to that of as-cast. Nematollahi, et al. [259] investigated the influence of PBF-LB/M process parameters on the fabrication of NiTiHf alloy. The result demonstrated that, low volumetric LE and high scanning speed prevent or significantly decrease the undesigned pore formation. In another study, low LE was found to facilitate the lack of grains fusion and poor powder bed spreading in the subsequent layers, which resulted in a highly porous BMG part [260]. During PBF-LB/M, oxygen is mostly absorbed by the powders. Thus, most AMed BMG parts contained oxygen contamination. However, the oxygen content depends on the alloy reactivity. For instance, Fe-based are less susceptible when compared to Zr-based BMG. Oxygen contributed to the formation of HAZ and hence, more crystallization in PBF-LB/M processed BMGs [211, 261]. High oxygen content was reported to not only degrades the toughness and ductility, but also increases the porosity of the PBF-LB/M processed BMG [262]. Various 3D printed scaffolds and implants with designed and controlled interconnected network of pores are presented in Figure 10.
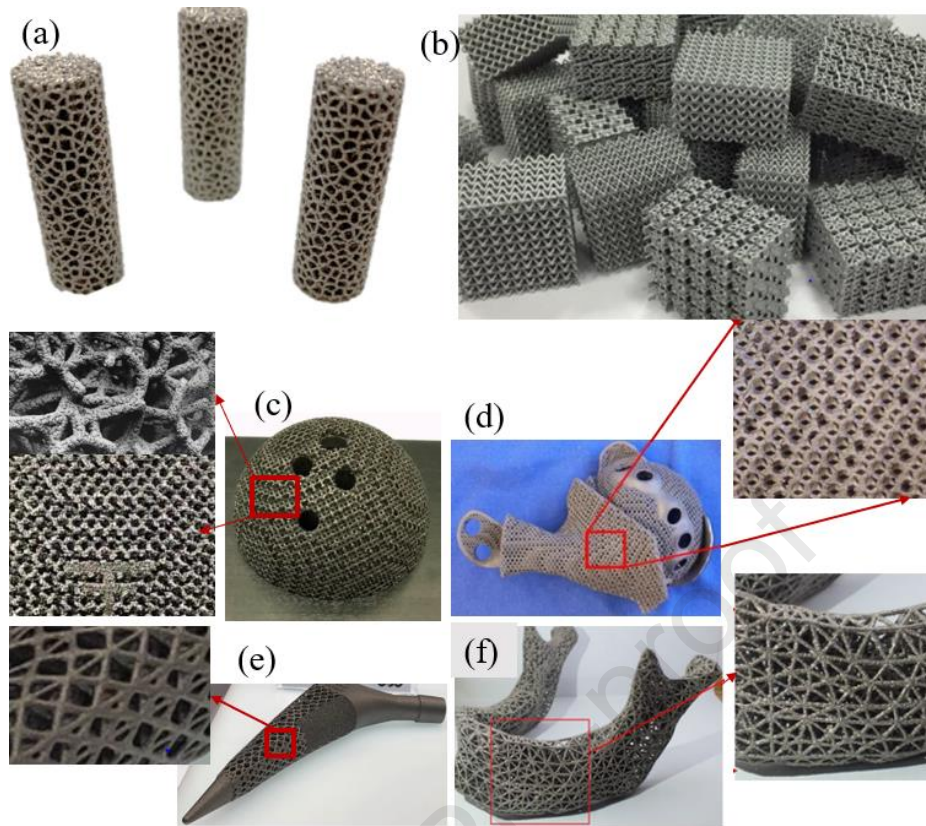
Figure 10: Variety of additively manufactured scaffolds and implants with designed and controlled interconnected network of pores developed through different unit cells (a) cylindrical lattice structure [263] (b) cubical lattice structure [264] (c) acetabular hip cup [263] (d) acetabular reconstruction custom implant containing flanges, solid plate, and an acetabular cup with screw holes for fixation [265] (e) hip stem implant [266] (f) mandibular prosthesis scaffold [267]

3.4.2 Influence of PBF-LB/M process parameters on microstructure and crystallisation

To control the properties of the 3D printed BMG parts, it is crucial to understand the mechanisms of macrostructural evolution in amorphous alloys during PBF-LB/M. The microstructure and the phase formation of the BMGs processed through PBF-LB/M can efficiently be tailored if the PBF-LB/M processing parameters are properly designed and controlled. Thus, a novel BMGs with desirable properties for specific functions can be fabricated. The initial search of PBF-LB/M process parameters to fabricate FeCrMoCB BMG resulted in extreme fragility, pronounced cracking and subsequent failure of the BMGs

specimens (Figure 11) [196]. Despite improvement in the optimisation of PBF-LB/M parameters for processing of BMGs, the formation of crystalline phases still persists, especially when high LE is used [268]. A fully amorphous BMG with less microstructural defects is formed when lower LE is used, while higher energy resulted in serious crystallization [106]. The effect of LE on structural evolution is investigated by Ouyang, et al. [269], and found that, crystallisation within the microstructure is induced by high LE while the amorphous phase volume fraction is reduced. The effect of the LE, laser power and laser speed on the amorphous formation during PBF-LB/M of Fe-based BMG is presented in Figure 12 [270].
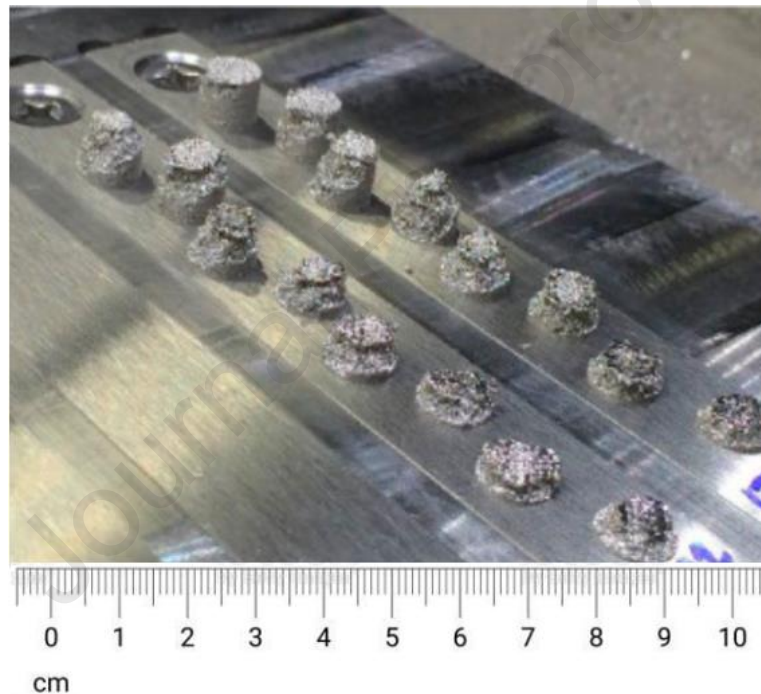

Figure 11: Photograph of the FeCrMoCB BMG specimens processed during initial parameters selection
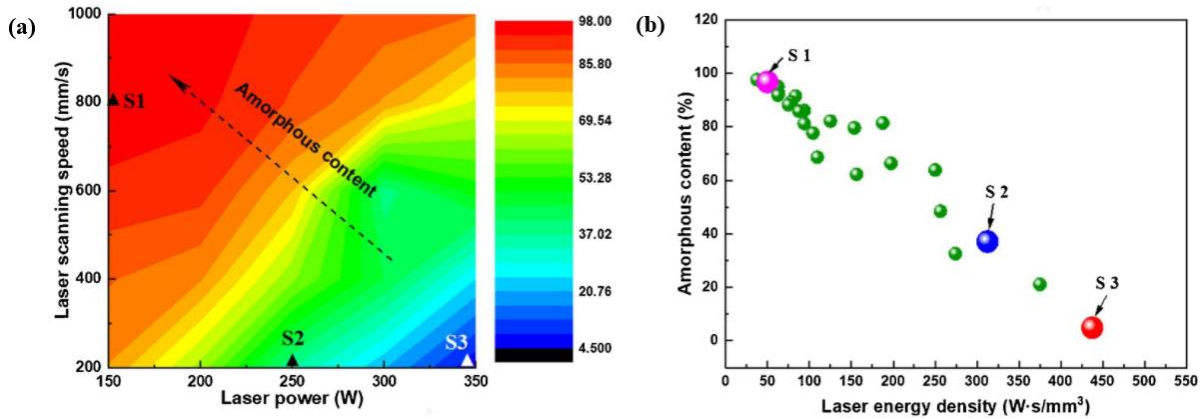
Figure 12: Influence of process parameters on amorphous contents of the Fe-based BMG processed through PBF-LB/M process (a) A map relating scanning speed, laser power and amorphous contents (b) LE verses amorphous contents

Another parameter, which has very strong influence on the microstructure, porosities and crystallization of the BMGs fabricated via PBF-LB/M techniques is the scanning strategy [240, 271, 272]. To improve the defect distribution and decrease the porosities, unidirectional scanning strategy rotated in the adjacent layers by a specific degree is employed. To investigate the defect formation, normally a single melting (unidirectional scanning vectors) is used [253]. The powder is fused from the outer to the central part of the processed BMG component through off-set strategy. A chessboard also called island strategy is employed to relieve the thermal stresses and modify the microstructure of the fabricated BMG parts [271, 273]. Double melting (re-melting) scanning strategy played a significant role in modifying the thermal history, microstructure and the amorphisation, without compromising the relative density [274]. A study conducted by Żrodowski, et al. [275] and Nam, et al. [276] revealed a poor amorphisation during preliminary laser melting, while the glass-forming of Fe-based alloy significantly increased during the re-melting. Thus, it can be concluded that, scanning strategy is the powerful tool for modifying the microstructure, size and the defect distribution and manipulating the material properties.

3.4.3 Influence of process parameters on balling formation during PBF-LB/M of BMG

Balling is a particular defect, which occurred during PBF-LB/M by inability to wet the previous layer due surface tension. It reduces the quality of the final PBF-LB/M processed parts by frustrating the formation of continuous melt lines and resulted in rough, and spheroidal bead surfaces [277]. Additionally, balling may result in severe cases by aggravating in the successive layers, thereby causing power to jam the coating mechanism. Other disadvantages of balling formation on the PBF-LB/M processed part include formation of highly rough surface, pores between the discontinuous metallic balls, which hinder the movement of paving roller, especially when the balling is severe [278]. To reduce balling effect during PBF-LB/M, low scanning speed, high power or modest LE should be used [250, 279]. Moreover, maintaining oxygen levels at 0.1 % or employing re-melting strategy significantly suppress the balling formation [279].

3.5 Laser powder-bed fusion of biomedical BMGs

The materials to be used for the repair or replacement of hard tissues such as bone are expected to be completely non-toxic, highly biocompatible and possess bone-match mechanical behaviours. In recent years, there is rising interest in the use of BMGs as biomaterials (biomedical BMGs), especially for the repair/replacement of bones due to their unique properties [65, 165, 280, 281]:

- Extreme hardness, high-strength and resistance to wear; thus, it is foreseen as an excellent biomaterial for load-bearing areas.

- Superior corrosion resistance: thus, it does not easily release ions to the body fluid and less prone to pitting corrosion after implantation.

- Good biocompatibility and osteointegration, especially when toxic elements-free BMG is synthesised, and its surface tailored to allow sufficient tissue adhesion.

- Exceptional thermoplastic formability: thus, it allows fabrication of different shapes and structures.

However, the processability of biomedical BMGs is challenging through conventional techniques, due to its high brittleness and hence, unable to form large BMG size beyond 50 mm, despite the presence of high glass-forming and toxic elements (Ni and Be) in the alloy. PBF-LB/M is a size limitless novel technique, which is expected to solve these problems. Based on the available literature, the PBF-LB/M of biomedical BMGs so far reported include three different BMGs, which are based on Zr, Fe and Ti. These systems of BMGs are mainly used for the synthesis of bone implants and scaffolds due to their outstanding functional, physical, mechanical and biomedical behaviours. Various bioactive, biocompatible and complex BMG parts with geometries exceeding the critical casting size were produced through PBF-LB/M [134, 202, 282]. Based on the current literature, the use of PBF-LB/M to fabricate biomedical BMGs have so far recorded the following success.

- The lasers in PBF-LB/M have sufficient energy to melt biomedical BMGs that are of Zr-, Fe- and Ti-based [126, 139].

- The cooling rate of PBF-LB/M is sufficient to produce fully amorphous BMGs, even with poor glass forming alloys [134].

- BMGs components with a wide range of geometries and larger sizes than those produced via pre-existing conventional techniques can easily be manufactured through PBF-LB/M technique [283, 284].

- PBF-LB/M can be used to combine two different phases (crystalline and amorphous) within a single component, which is proven to enhance the fracture toughness and ductility of the biomedical BMG [40, 285].

- Unlike conventional BMG processing techniques, various alloy compositions can be formed through PBF-LB/M processes, even those with low GFA. However, severe crystallization maybe observed (Table 2) [275].

Table 2 BMGs fabrication through PBF-LB/M processes of some low GFA alloys which cannot be achieved via conventional techniques

BMGs	Remarks	Refs.
$Fe_{71}Si_{10}B_{11}C_6Cr_2$	Despite high crystallisation, the amorphous structure is restored by Point-Random rescanning strategy. Proper parameters optimisation is proposed to reduce the crystallisation	[275]
$Al_{86}Ni_6Y_{4.5}Co_2La_{1.5}$	Severe crystallisation occurred in both HAZ and the edge of the melt pool due to thermal fluctuation at high laser power. Selecting appropriate laser power is expected to reduce the crystallization	[136]
$Al_{86}Ni_6Y_{4.5}Co_2La_{1.5}$	Severe crystallisation observed due to poor heat transfer from the support to the substrate which resulted in decrease in the actual cooling rate. High substrate temperature is expected to reduce the crystallization	[286]
Ti6Al4V (Ti64)	Partially crystallised with MG nanobands and β-grans	[287]
$(Ti_{0.65}Zr_{0.35})_{90}Cu_{10}$	Crystalline phases presence in the HAZ. Alloy composition need to be optimised to achieve improved mechanical properties and size.	[234]

3.6 PBF-LB/M of biomedical BMG systems

Several systems of biomedical BMGs with different elemental compositions were processed through PBF-LB/M techniques [133, 288]. In this paper, the authors focused on BMGs systems processed through PBF-LB/M, specifically for biomedical applications, herein referred to as biomedical BMGs. Figure 13 shows the articles breakdown published from 2012 to date on biomedical BMGs processed through PBF-LB/M techniques. It could be seen that PBF-LB/M of Zr-based BMGs were the most published articles. Out of 308 published articles, it accounts for about 60 %, while the remaining 40 % shared to Fe-based BMGs with 37.39% and Ti-based BMGs with only 2.61 %. Figure 14 displayed some PBF-LB/M processed biomedical Zr-based BMG.
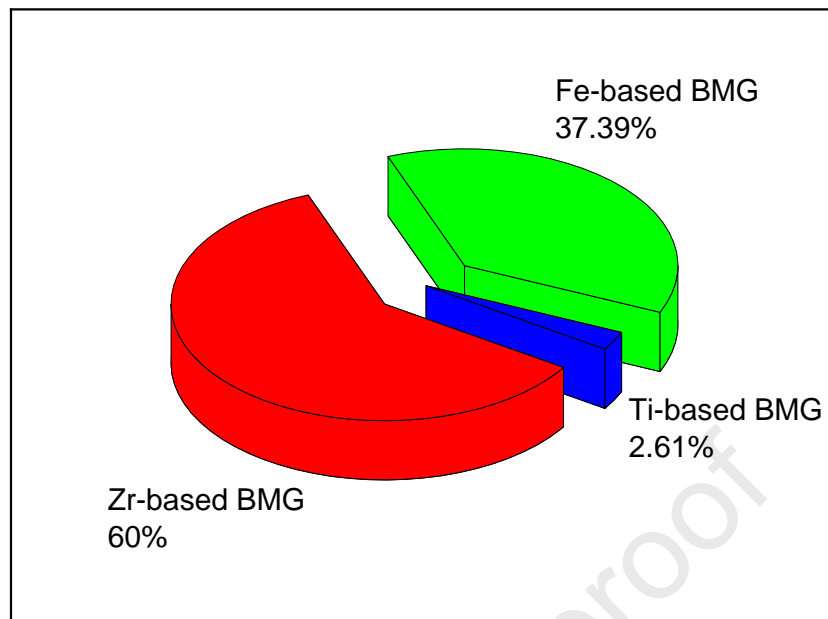
Figure 13: Articles published on PBF-LB/M of biomedical BMGs. The data is based on research publications on Zr-, Fe- and Ti-based BMGs in Google Scholar database. The keywords used are; Zr-, Fe-, Ti-based, BMG, laser, additive manufacturing
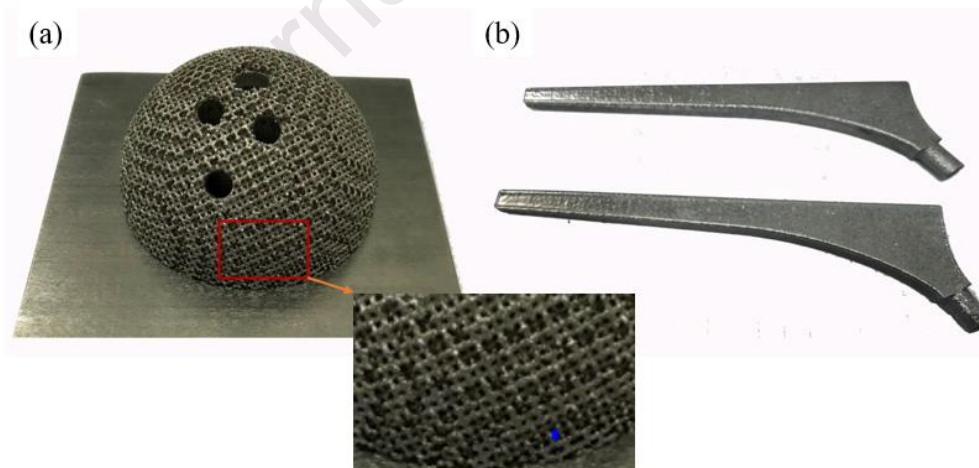
Figure 14: Zr-based BMG 3D printed implants fabricated by PBF-LB/M process (a) acetabular cup with corresponding pores topology (b) femoral components [289]

3.6.1 Processability of Zr-based biomedical BMGs through PBF-LB/M

PBF-LB/M is proven as a viable candidate for processing Zr-based BMGs with mechanical and biomedical behaviours comparable to BMGs processed through conventional techniques.

The advantage of PBF-LB/M in processing BMGs over the conventional techniques is that, its process parameters or strategies can be tailored to suit a specific property or functional requirement. For instance, scanning a layer twice reduces the composition segregation, thereby enhancing the amorphous fraction of the BMG [236]. A fully dense $Zr_{52.5}Cu_{17.9}Ni_{14.6}Al_{10}Ti_5$ BMG scaffold was fabricated and found that, the laser power has major influence in achieving dense BMG. Additionally, the porosities could be decreased with the increase in the scanning energy [290]. However, some mechanical properties must be compromised. Some Zr-based BMGs processed through PBF-LB/M were reviewed and presented in Table 3.

Table 3 Critical review of some biomedical Zr-based BMGs processed through PBF-LB/M

Chemical composition (%)	Outcomes	Limitations	Ref.
$Zr_{57.4}Ni_{8.2}Cu_{16.4}Ta_8Al_{10}$	BMG was 3D printed with enhanced toughness and plasticity due to Ta addition with >90% amorphous. No microcracks	Ta added do not melt due to extreme melting Temperature (Tm = 2995°C)	[291]
$Zr_{52.5}Cu_{17.9}Ni_{14.6}Al_{10}Ti_5$	BMG produced with good wear and corrosion resistance	Prematurely failed plastically due to residual pores. Require proper parameters optimization	[292]
$Zr_{59.3}Cu_{28.8}Nb_{1.5}Al_{10.4}$	Fully amorphous BMG developed	Inherent porosities in the printed part Un-molten powder presence in printed BMG	[255]
$Zr_{59.3}Cu_{28.8}Nb_{1.5}Al_{10.4}$	Fully amorphous and cracks-free BMG was produced from alloy with low GFA	Cannot cast to for 0.5 mm parts, oxygen contents deteriorate GFA. Low toughness due to porosities	[198]
$Zr_{59.3}Cu_{28.8}Nb_{1.5}Al_{10.4}$	BMG produced has lower fracture toughness than the as-cast samples. Fully amorphous and cracks-free	BMGs smaller than as-cast	[293]

$Zr_{55}Al_{10}Ni_5Cu_{30}$	In the 1st and 2nd layers, fully amorphous is formed. Partial crystallisation start after 2nd layer.	Partially crystallised at HAZ	[107]
$Zr_{52.5}Ti_5Cu_{17.9}Ni_{14.6}Al_{10}$	Large scale, complex and fully dense crack-free Zr-based BMG formed.	High LE resulted in high cooling rate deteriorate the chemical heterogeneity of the melt pool and hence severe crystallisation	[106]
$Zr_{55}Cu_{30}Al_{10}Ni_5$	Crack-free Zr-based BMG with significant structural heterogeneities, fully amorphous in molten pool	Partially crystallised with nanocrystals in the HAZ.	[229]
$Zr_{52.5}Cu_{17.9}Ni_{14.6}Al_{10}Ti_5$	Fully amorphous scaffold was produced	High porosities obtained reduces the plastic strain. High LE used compromised the vitrification	[290]
$Zr_{60.14}Cu_{22.31}Fe_{4.85}Al_{9.7}Ag_3$	Fully amorphous Zr-based BMG produced have good biocompatibility and cell proliferation comparable to the commercial Ti6Al4V implant	BMG fabricated smaller than critical casting size	[133]
$Zr_{58.5}Cu_{15.6}Ni_{12.8}Al_{10.3}Nb_{2.8}$	Zr-based metallic glass forming powder successfully deposited on both amorphous and crystalline substrates of the same nominal composition	Crystalline in the HAZ formed due to residual heating of the unmelted substrate below the melt zone and incomplete heating.	[294]
$Zr_{52.5}Ti_5Al_{10}Ni_{14.6}Cu_{17.9}$	Nearly fully dense BMG with micro-hardness, tensile strength and flexural strength comparable to the as-cast BMG parts.	Partially crystallised, though not highly crystalline and mechanical properties not deeply affected	[125]
$Zr_{52.5}Cu_{17.9}Ni_{14.6}Al_{10}Ti_5$	Viscous flow of the specimens fabricated by LAM is like that of copper mould casted BMG.	Porous and partially crystallised	[295]
$Zr_{59.3}Cu_{28.8}Al_{10.4}Nb_{1.5}$	The LAM processed BMG shows outstanding mechanical properties like high hardness, wear resistance, and compressive and flexural strength	Formation of nanocrystals in the HAZ due insufficient cooling rate to bypass crystallisation.	[296]

33

3.6.2 Processability Fe-based biomedical BMGs through PBF-LB/M

The use of Fe-based BMGs as biomedical material is extensively studied due to their excellent properties such as high strength, high hardness and considerably low cost [104, 297]. Aside high GFA of Fe-based BMGs, they have reasonable biocompatibility, excellent corrosion and wear resistance [298, 299]. Several research focusing on PBF-LB/M of Fe-based BMGs were reported, which were critically reviewed and summarised in Table 4.

Table 4 Critical review of some biomedical Fe-based BMGs processed through PBF-LB/M

Chemical composition (%)	Outcomes	Limitations	Ref.
$Fe_{55}Cr_{25}Mo_{16}B_2C_2$	Fully amorphous BMG with size larger than critical casting size and enhanced mechanical properties is produced	Some part of the processed specimen experienced low temperature (Tg)	[300]
$Fe_{54.35}Cr_{18.47}$	BMG with near fully amorphous formed	Partially crystallised. Lower LE unable to fully melt powder resulting in pores and cracks from thermal stress Low hardness	[234]
$Fe_{74}Mo_4P_{10}C_{7.5}B_{2.5}Si_2$	Highly complex BMG scaffold produced	Partially crystallised, cracks, rough and porous BMG developed	[255]
$Fe_{68.3}C_{6.9}Si_{2.5}B_{6.7}P_{8.7}Cr_{2.3}Mo_{2.5}Al_{2.1}$	Fully amorphous BMG produced with identical crystallisation and intrinsic magnetic behaviour to that of initial BMG powder.	Partial melting of powders and highly porous microstructures due to insufficient LE. Only few SLM parameters studied	[241]
$Fe_{43.7}Co_{7.3}Cr_{14.7}Mo_{12.6}C_{15.5}B_{4.3}Y_{1.9}$	The propagation of micro-cracks from the micro pores due to thermal stresses developed during SLM of F-based BMG is ascertained.	Partial crystallisation, numerous pores and micro-cracks	[301]
$Fe_{43.7}Co_{7.3}Cr_{14.7}Mo_{12.6}C_{15.5}B_{4.3}Y_{1.9}$	The volume of amorphous fraction reduced, and crystallisation induced due to high LE used.	Partially crystallised and cracks formed due to high LE. Low LE might be better but susceptible to porosities and unmelted powder in the BMG	[270]

34

$Fe_{71}Si_{10}B_{11}C_6Cr_2$	First melting resulted in poor glass formation when SLM of Fe-based BMG. Novel scanning strategy (second melting) enhanced the glass formation	Partial crystallisation, highly optimised scanning strategy may avert this problem	[275]
$Fe_{73.7}Si_{11}B_{11}C_2Cr_{2.28}$	The voids generated due to partial melting of powders were effectively filled when scanned twice and enhanced reflow of melt pool	Partial crystallisation, highly optimised scanning strategy may avert this problem	[276]

3.6.3 Processability Ti-based biomedical BMGs through PBF-LB/M

For decades, the use Ti and its alloys in the biomedical field is being reported [302]. Their outstanding mechanical properties like high strength, good corrosion and wear resistance, coupled with commendable biomedical behaviour such as good biocompatibility and osteointegration, lead to their widespread acceptability as biomedical materials, especially for the repair or replacement of hard tissues [159]. Considering the unique properties of amorphous alloys, Ti-based BMGs are expected to outweigh its crystalline counterpart in terms of mechanical and biomedical characteristics. Therefore, its applicability as biomaterials and processability is exploited by many authors [20, 303]. The pre-existing BMG fabrication techniques could not produce sufficient size for the industrial applications, especially when toxic elements (Ni and Be), which are proven to have high GFA are removed from the alloy. Till date, 50 mm is the highest geometrical size achieved by these techniques [304]. Optimizing the alloy composition and the emergence of PBF-LB/M is expected to overcome this limitation. The Ti-based BMG processed through PBF-LB/M were critically analysed and summarized in Table 5.

Table 5 Critical review of some biomedical Ti-based BMGs processed through PBF-LB/M

Chemical composition (%)	Outcomes	Limitations	Ref.

Ti$_{47}$Cu$_{38}$Zr$_{7.5}$Fe$_{2.5}$Sn$_2$ Si$_1$Ag$_2$	Fully amorphous BMG with good thermal stability, high compressive strength and high density achieved.	Compared to as-cast rods, the fabricated Ti-based BMG failed prematurely	[135]
(Ti$_{0.65}$Zr$_{0.35}$)$_{90}$Cu$_{10}$	Compared to BMGs processed by conventional techniques, the SLM processed BMG have finer and coarse microstructure	Crystalline phases presence in the HAZ. Alloy composition need to be optimized to achieve improved mechanical properties and size.	[234]
Ti6Al4V (Ti64)	Crack-free and near-full dense Ti-based BMG composite formed. Addition of MG densified SLM processed Ti64 alloy	Partially crystallised with MG nano-bands and β-grans	[287]

3.7 Modelling and simulation of PBF-LB/M for fabricating BMGs

Recently, various researches were published on simulation of PBF-LB/M processes and analysing the laser-material relationship, crystallisation, pores, heat variation and cracks behaviour [305]. Panwisawas, et al. [306] studied the particle distribution and the thermal fluid flow during PBF-LB/M of Ti alloy using simulated and experimental approaches. The model developed for the thermal fluid flow revealed an irregular-shaped single laser scanned tracks when scanning speed and the powder layer thickness are increased. In a similar study, increase in laser speed was found to transform the shape of the pores from near-spherical to elongated shape. According to computational fluid dynamics, pore-shape change occurred due to change in pattern in the melt pool [307]. Gürtler, et al. [308] developed the model simulation of laser beam melting (LBM), which described the melting, solidification and wetting phenomena during LBM. The model revealed the fundamental properties of the LBM. The crystallisation behaviour in the HAZ during PBF-LB/M of BMGs was studied through molecular dynamics (MD) simulation [309]. It was found that the relaxation time between the glass transition and maximum heating temperatures determine the crystallisation rate. At first heating and cooling

processes, crystallisation occurred, and the rate of crystallisation is inconsistent at various temperature rates (Figure 15). To ease computational difficulties during modelling and MD simulation of the PBF-LB/M processes in determining the crystallisation behaviour, Lindwall, et al. [310] and Lindwall, et al. [231] developed a simplified simulation approaches with about 0.2 % less time and about 1,000 fold efficiency rise. It is revealed that crystallisation occurs at the solidified melt pool under the heat source (lower layers of the heating layer).
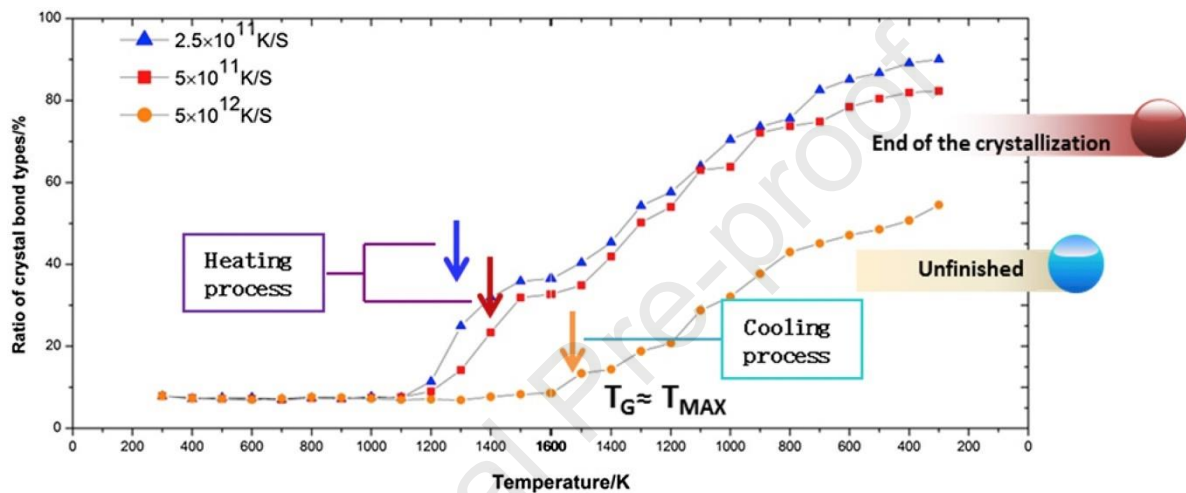
Figure 15: Illustration of crystallisation behaviour first heating and cooling process at various rates of temperature for the different crystal bonds

4. Mechanical properties of BMGs

The amorphous nature of BMGs bestowed its unique mechanical, physical and biomedical behaviours. For this reason, there has been a widespread quest for its applications in various fields, especially in the biomedical field. Thus, with recent growing interest in BMGs, it is anticipated that biomedical BMGs will soon dominate the currently used crystalline biomaterials, especially if the substantial geometrical size is achieved. Unlike crystalline solids, BMGs have no translational long-range order, grain boundaries and dislocation-mediated crystallographic slip or plastic deformation. Therefore, the whole atoms move when the load is applied, leading to elastic deformation. Hence, BMGs can withstand a very high load without failure. Thus, BMGs have unique physical and mechanical properties such as high strength and

hardness, high elasticity, excellent resistance to corrosion and wear. This exceptional property of BMGs makes them potential candidate for biomaterials, especially for the repair/replacement of hard tissues. Table 6 compares the mechanical properties of the commercial vit 105 BMG, cortical bone and the most commonly used crystalline biomaterials.

Table 6 Mechanical properties of the commercial vit 105 BMG, cortical bone and the crystalline biomaterials [311, 312]

Property	316L SS	Co-Cr-Mo	Ti-6Al-4V	Vit 105 BMG	Cortical bone
Elastic Modulus (GPa)	193-210	210-255	101-129	90	3-50
Density (g/cm^3)	7.9	8.3	4.4	5.9	0.7-1.85
Tensile strain to Failure (%)	12-40	8-28	8-15	<1	2
Tensile yield strength (MPa)	690-690	450-1030	760-1050	1,900	130-150
Toughness (MPa/m	100	-	65-92	55-60	3.2-8.0
Elastic limit (%)	0.34	0.81	0.67	2.0-2.2	1
Fatigue limit at 10^7 cycles (MPa)	200-800	207-970	598-816	910	20-60
Vickers Hardness (Kg/mm^2)	365	345-390	320	590	63-75

4.1 Strength, Modulus of Elasticity and Plasticity of AMed BMGs

The E of 70-95 GPa and the elastic limit of 2 % of the biomedical BMGs are comparably closer to that of the human bone (10-30 GPa and 1 %, respectively) than the crystalline biomaterials [313]. High elastic limit of the BMGs implies that, they can uniquely flex to elastic with the bending of human bones and therefore, the stresses are more uniformly distributed than the crystalline biomaterials. This resulted in faster healing rates by reducing the effect of stress concentration and minimising the stress shielding effect. Moreover, the BMGs-based screws implant can be made with a very thin shank and deep threads, thereby allowing a better holding power to the fractured human bones. Unlike conventional 316L stainless steel, biomedical BMG-based stents need a lower cross-section of the strut (only one third), with a very much higher deflection (up to five times) [314]. With tensile yield strength of 1,900 MPa,

commercial vit 105 Zr-based BMG is almost twice and threefold that of Ti-6Al-4V and 316L SS, respectively [315, 316].

The processing approaches of BMGs played very vital role in its final mechanical properties. For instance, unintentional micro-porosities are hard to ignore on the additively manufactured BMG parts [139]. This resulted in an interconnected micro-cracks, which significantly degrades the strength of the BMG parts, especially under loading condition [139]. However, in most instances, the strength and plasticity of the AMed BMGs resemble or are even higher than those conventionally manufactured (casted). Zhang, et al. [133] fabricated a Ni-free Zr-based biomedical BMGs through PBF-LB/M technique. All the 3D printed specimens were found to have higher yield strength of about 1700 MPa and lower E (79 GPa) than the as-cast BMGs, with values 1557 MPa and 84 GPa, respectively. Another study revealed a slightly lower value of yield strength (1504 MPa) and E in the AMed parts compared to as-cast counterpart [228]. Like BMGs produced through conventional methods, PBF-LB/M processed BMGs are brittle, most of them exhibit little or no plasticity. To enhance the strength and plasticity of the PBF-LB/M processed BMGs, researchers proposed chemical alloying, which resulted in the formation of the second phase [287, 317]. Li, et al. [289] introduces Cu and Cu-Ni alloy as a second phase to suppress the micro-cracks, which normally formed during the fabrication of BMGs. This not only significantly rise the strength, but also the plasticity of the PBF-LB/M processed BMGs [228].

4.2 Fracture toughness of AMed BMGs

BMGs are generally referred to as quasi-brittle materials, which are tougher than native (oxide) glasses. The fracture toughness of BMGs is not fully understood. It varies between the BMGs types, depending on the alloy combination, processing technique and the type of test used [318, 319]. The toughness of some BMGs is comparable to that of Ti-alloys while some

are highly brittle like that of silicate glasses [318]. The stress-strain curve comparing the PBF-LB/M processed and as-cast BMGs is depicted in Figure 16a.

The heating involved during PBF-LB/M process resulted in the formation of a brittle intermetallic layer in the HAZ, which makes the AMed BMGs more brittle than the as-cast counterparts [174]. Several approaches to improve the AMed BMGs were proposed. The most common is by introducing a tough phase into the BMG matrix to form a BMG composite [289, 291]. Another approach is by careful control of the defects such as micro porosities and crystallization fractions during PBF-LB/M of BMGs (Figure 16b). This resulted in the micro-pores induced shear banding, which retards the crack propagation and hence, improves the fracture toughness and plasticity of the PBF-LB/M processed BMGs [320].
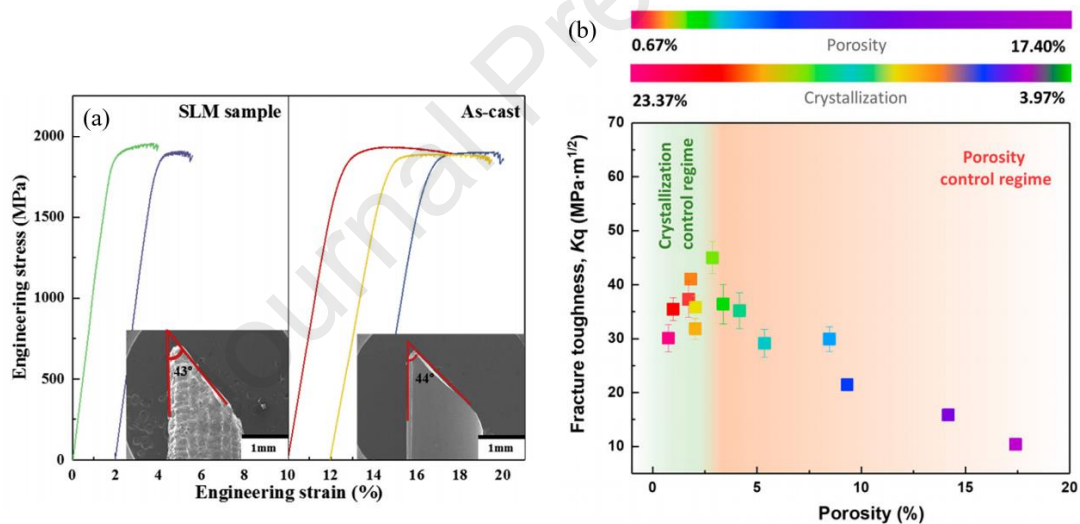
Figure 16: PBF-LB/M processed BMGs (a) compressive stress-strain curve and the plane of fracture compared with the as-cast BMGs (b) fracture toughness at different crystallization fractions and porosities [291, 320]

4.3 Bio-mechanical Behaviour of BMGs

Recently, BMGs were specially developed for biomedical use. This is due to their proven outstanding properties like high strength, relatively low modulus of elasticity, good biocompatibility, high resistance to failure and good corrosion resistance when compared with

the currently used crystalline metallic alloys, like Ti6Al4V. The wear behaviour of 3D printed BMG observed in simulated body fluid at 37° revealed a higher resistance to wear than the Ti6Al4AV alloy (Figure 17a). Several *in-vitro* studies aimed to evaluate the feasibility of BMGs as potential biomaterials were reported [133, 321]. Although not yet at a commercial level, various biomedical BMG devices and implants were designed and fabricated. An *in-vitro* biocompatibility investigation on PBF-LB/M processed BMG was carried out and the results compared to that of as-cast BMG and Ti6Al4V alloy. The MG63 cells seeded in 96 well-plates revealed a higher proliferation and hence, better growth profile on the 3D printed BMG than the Ti6Al4V alloy as shown in Figure 17b. When compared with 316L stainless steel, various types of 3D printed Fe-based BMGs seeded in SAOS2 cells shows much higher cells viability (Figure 17c) [321]. This confirmed the good biocompatibility and biosafety of the 3D printed BMGs compared to crystalline alloys. The A375 cells cultured on 3D printed BMG are densely distributed and better spread on the 3D printed BMG than the crystalline Ti6al4V (Figure 18a-c) [133]. The adhesion test conducted using MC3T3-E1 cells on AMed Zr-based BMG (AMLOY ZR01), as-cast Zr-based BMG (AMLOY ZR01) and Ti-6Al-4V substrates shows a dense layer on the surface of each material after Day 7. This confirmed the support of osteoblast cells growth and adhesion of 3D printed BMG comparable to that of commercial grade Ti-alloy (Figure 19).

Zhang, et al. [133] compared the biocorrosion resistance of the PBF-LB/M processed BMG, as-cast BMG and the commonly used Ti6Al4V implants through electrochemical potentiodynamic polarization measurements in a simulated body fluid. The 3D printed BMG was revealed to have lower passive densities in the passivation region as depicted in Figure 20. This shows that, PBF-LB/M processed BMG have better corrosion properties than the as-cast BMG and crystalline Ti6Al4V alloy.
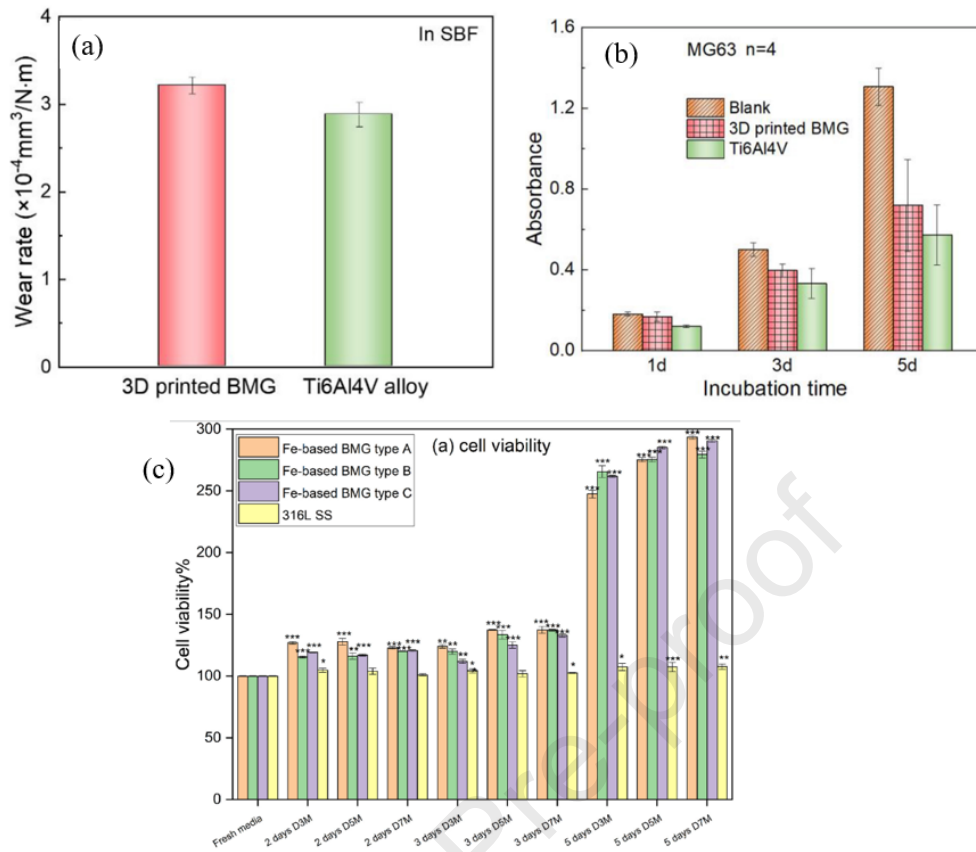
Figure 17: (a) Wear rate of 3D printed BMG and Ti6Al4V alloy observed at 37° in a simulated body fluid (b) Cytotoxicity test of 3D printed BMG and Ti6Al4V alloy using MG63 cell showing the level of absorbance for 1 – 5 days (c) cells viability of three different types of 3D printed Fe-based BMGs compared to 316L stainless steel cultured in SAOS2 cells media for 2, 3 and 5 days [133, 321].
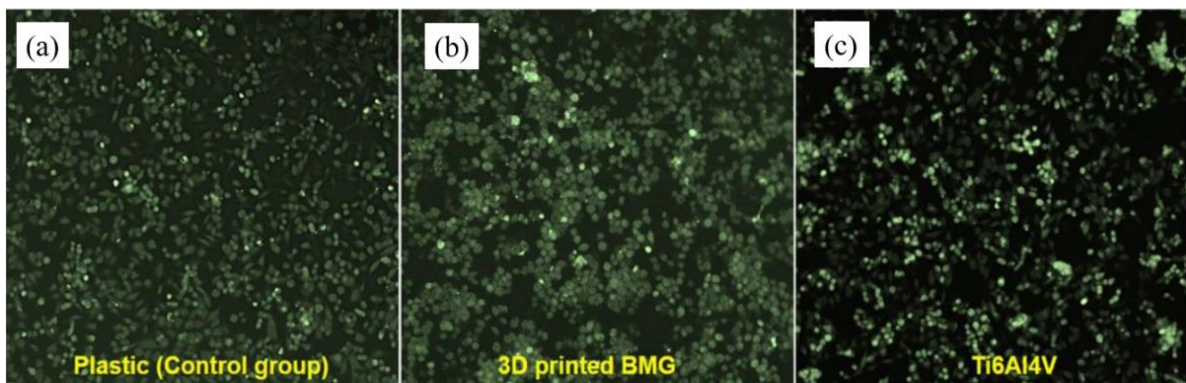
Figure 18: Cells morphology showing the cells distribution and density of (a) control group (b) 3D printed BMG and (c) Ti6Al4V alloy seeded for 24 hours.
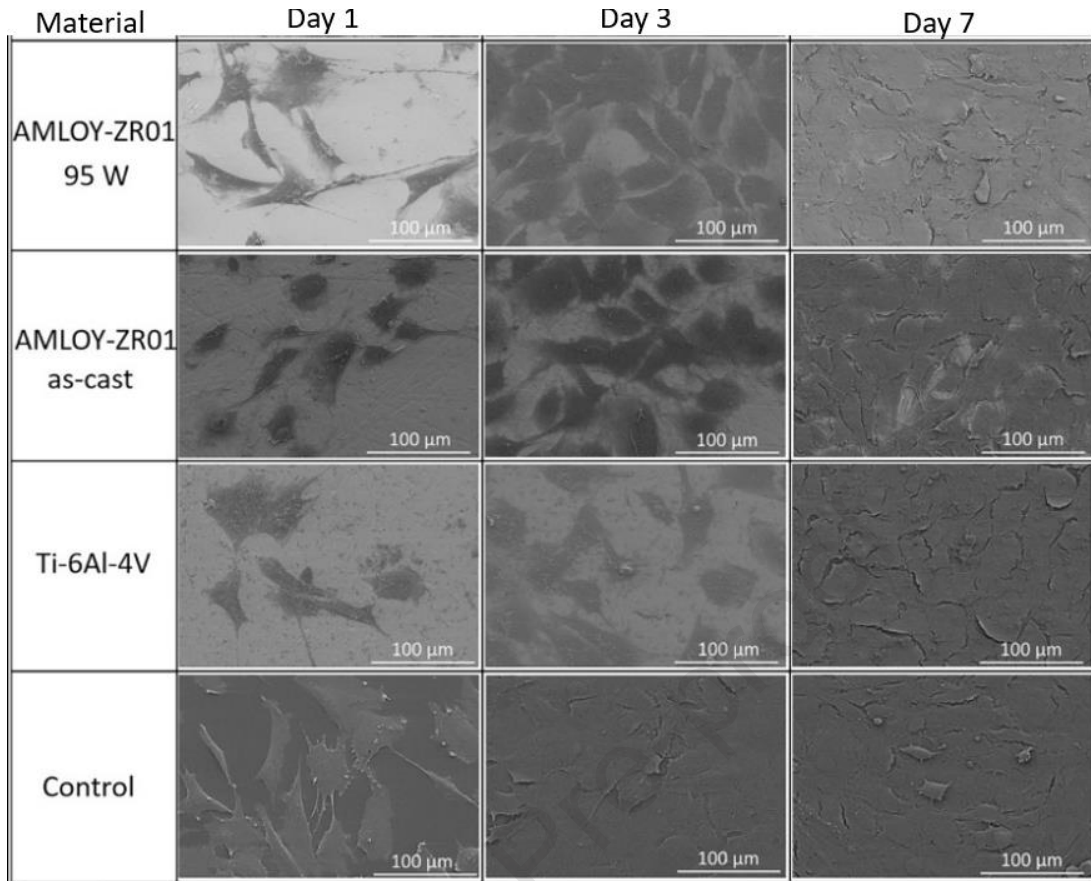
Figure 19: SEM micrographs showing the MC3T3-E1 cells adhesion and proliferation on 3D printed Zr-based BMG (AMLOY ZR01), as-cast Zr-based BMG (AMLOY ZR01), Ti-6Al-4V alloy and control substrate surfaces, seeded for Day 1, 3 and 7 [322].
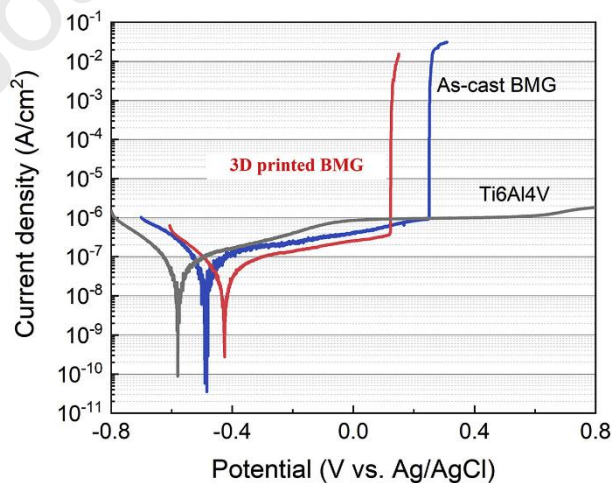
Figure 20: Electrochemical polarization curves of PBF-LB/M processed BMG specimens at 37°C in simulated body fluids compared to as-cast BMG and Ti6Al4V alloy [133].

5. Current challenges and future research perspectives

Nowadays, AM played a significant role in fabricating complex geometries, cost effective and patient-specific implants. Among the AM processes, PBF-LB/M has the greatest potentials in processing biomedical BMG implants. Unlike conventional BMG processing techniques, which were well established, PBF-LB/M of biomedical BMGs is still at its infant stage. There are numerous challenges that need to be addressed before the PBF-LB/M processed BMG implants fulfil the clinical requirements and meet the widespread acceptability. The most common challenges are partial crystallisation, which alters the initial properties of the BMGs, undesigned pores formation, which degrades the BMGs quality and microcracks, which propagated from the pores and lead to subsequent implant failure. To further satisfy various clinical requirements, future research on PBF-LB/M of BMGs should focus on optimising the process parameters, post-processing of PBF-LB/M processed BMG components, PBF-LB/M of BMG composite, developing biocompatible alloys with high GFA and control of residual stresses. The current challenges and future research trends are illustrated in Figure 21.
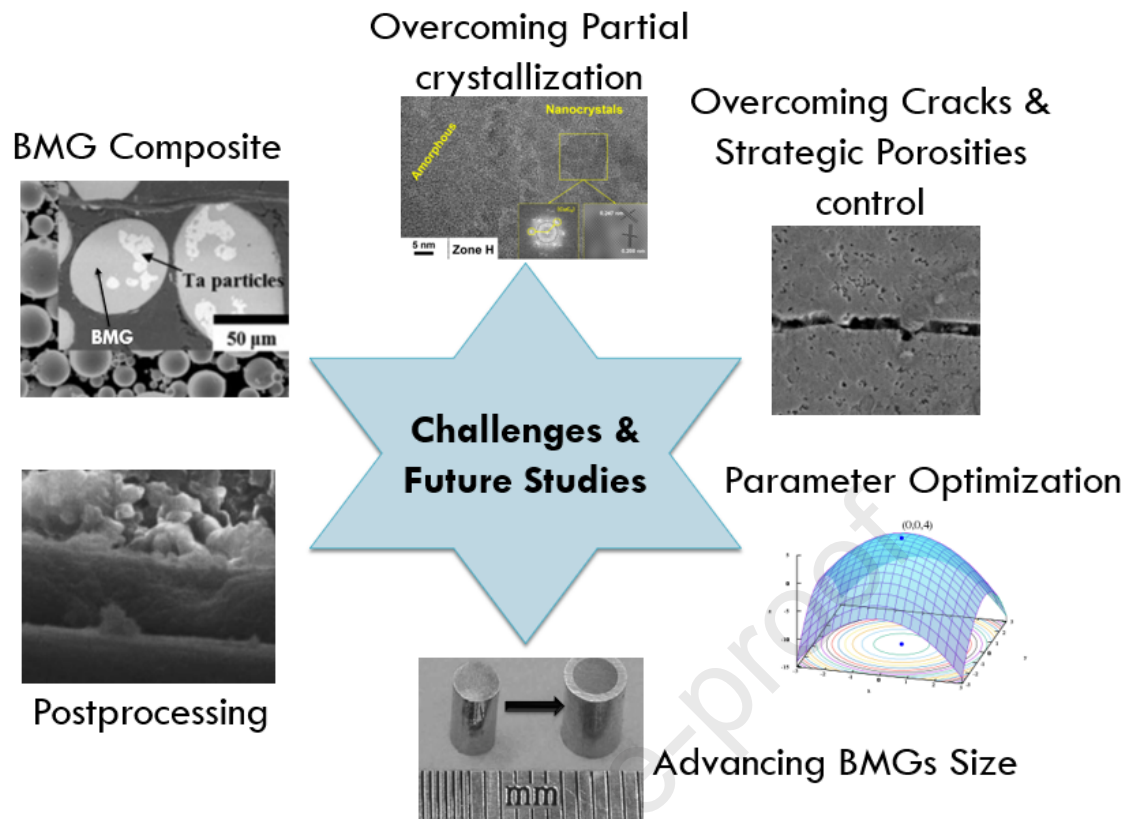
Figure 21: Illustration of current challenges and future research directions for PBF-LB/M of biomedical BMGs

5.1 Overcoming partial crystallisation

PBF-LB/M AM processes is characterized by complex thermal history, which resulted in accumulation of residual stresses and formation of crystalline phases in the HAZ during the BMGs processing [323, 324]. Thus, crystallization remained the critical and obvious challenge of BMG processed through PBF-LB/M approach. Thermal cycling coupled with long thermal exposure is the main cause of crystallization during 3D printing BMGs [196]. Pacheco, et al. [211] compared the thermal stability and crystallization of the as-cast and PBF-LB/M processed BMGs. The crystallization kinetics in the as-cast BMGs differs to that of PBF-LB/M processed due to structural relaxation molten pool and nano-crystals formation in the molten pool and HAZ, respectively. Aside the difference observed in the crystallization sequences, the crystallization of PBF-LB/M processed BMG occurred at lower temperature of about 440 °C

than the as-cast BMG, which occurred at 480 °C. Furthermore, the width of the supercooled liquid region of PBF-LB/M processed BMG specimens was found to be smaller than that of as-cast. Thus, it is quite difficult to bypass the formation of nanocrystals in the HAZ and partial crystallization phenomena in the BMG systems processed through PBF-LB/M and other AM processes [270, 310].

Partial crystallisation of BMGs resulted in properties deterioration of the 3D printed BMG components. Therefore, it cannot efficiently perform the required function [325]. There are various factors that contributed to the formation of partial crystallisation during PBF-LB/M of BMGs. As presented in Tables 3 to 5, most of the BMGs produced through PBF-LB/M partially crystallised. The major factors contributing to the crystalline phase formation during PBF-LB/M include: (i) lower LE or low power insufficient enough to melt the MG powder [234, 325] (ii) slow cooling rate, which is not fast enough to bypass crystallisation [269] (iii) poor material quality of the raw materials containing impurities, which has different or higher melting temperature than the MG powders [234] (iv) uncontrol heat treatment, which resulted in the formation of crystalline phases in the HAZ [228] and (iv) single scans strategy, which could not be able to melt the powder completely [275, 276]. Ouyang, et al. [269] investigated the factors that control the amorphous to crystalline phase transformation of two different 3D printed BMGs, and revealed the formation of higher amorphous phase in the BMG with low GFA (ZrAg) than those with high GFA (Zr55). Proper selection of finer MG powder and/or optimizing PBF-LB/M process parameters are expected to significantly reduce the problem of crystalline phase formation and hence, facilitate the amorphous formation during PBF-LB/M [241, 242]. The microstructure of the PBF-LB/M processed Fe-based BMG indicating the partial crystallisation and formation of nanocrystals is presented in Figure 22.
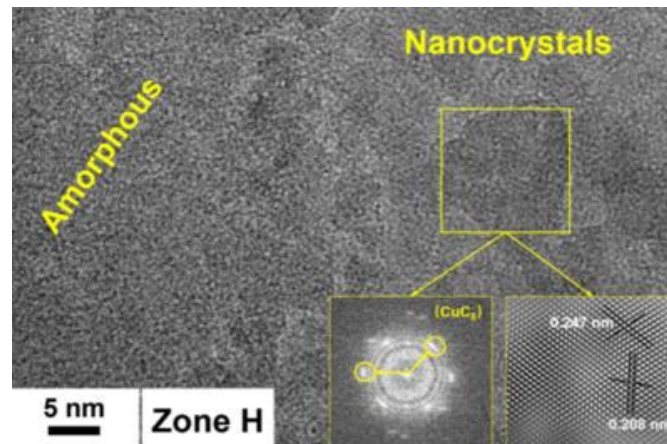
Figure 22: HRTEM micrographs showing microstructure of the partially crystallized Fe-based BMG processed PBF-LB/M indicating the amorphous and nanocrystals phases [289]

5.2 Overcoming cracks and strategic control of porosities

Microcracks formation is another strong issue, which need to be avoided during PBF-LB/M of BMGs. Most AMed BMG parts contained microcracks as presented in Tables 3 to 5. Microcracks and undesigned pores are defects formed in the 3D printed BMG implants, which significantly degrades its mechanical and biomedical behaviours [303, 326-328]. The presence of microcracks in the implants exposed them to a high corrosion rate and fretting damage. Low LE or low laser power may induce the formation of microcracks in the BMG parts due to inability to melt the powder sufficiently. Thus, resulted in a high porous structure and subsequent premature failure of the implants [136, 329].The formation of these microcracks during PBF-LB/M process is strongly attributed to thermal stresses, which accumulated due to high heat and fast cooling involved [330, 331]. The microstructural evolution and mechanism for the formation of microcracks in the Fe-based BMG processed through PBF-LB/M was studied by Ouyang, et al. [229]. It is revealed that cracks originated from the thermal stresses concentrated around the defects. These great challenges can be minimised or completely solved by optimising the PBF-LB/M process parameters/scanning strategy and/or employ a proper post-processing technique. Formation of micropores during PBF-LB/M process of BMGs

47

cannot be avoided due to high laser heat involved in the process. Porosities are needed in an implant for the sufficient tissue adhesion and growth. However, if not properly designed or controlled, it resulted in an interconnected or pores-induced microcracks, which degrades the mechanical properties of the AMed BMG part and resulted in its subsequent failure. A strategic defects control can enhance not only the strength, but also the plasticity and toughness of the PBF-LB/M processed BMG parts [319].

5.3 Optimising PBF-LB/M process parameters

Most of the BMGs processed through PBF-LB/M are not fully amorphous and contain some defects such as microcracks and porosities as seen in Tables 3 to 5. These defects are mostly related to inappropriate setting of the PBF-LB/M process parameters used in processing the BMGs. There is great challenge in down-selecting the parameters that best suit the fabrication of defect-free and fully amorphous BMGs. This is because, to achieve a specific requirement or property, other properties must be compromised. For instance, to fully melt the MGs powder, high LE has to be employed, but it resulted in an unstable melts pool [194] and the formation of less dense BMG. However, when the energy is too low, the powders will not be fully melted and hence, the formation of numerous pores and microcracks. Therefore, the optimum parameters must be set to accurately process BMGs through 3D printing with the required quality. To date, only two articles investigated the influence of PBF-LB/M process parameters on the processability of Zr- and Ti-based BMGs [241, 242]. These articles considered few parameters including scanning strategy, laser power and scanning speed. Yet, parameters like heat transfer, reflection, phase transformation, absorption and solid/liquid interface, which might have an influence on the laser radiation behaviour, are not considered [332]. Therefore, to fabricate BMGs with required accuracies and properties comparable to those produced through conventional methods, all factors should be given due consideration, for optimising the PBF-LB/M process parameters during biomedical BMGs processing.

5.4 Advancing the BMG size

Despite that, PBF-LB/M processes were able to fabricate larger BMGs size than those produced through conventional techniques, the size is still insufficient for the industrialisation and biomedical applications [196, 202, 300]. Moreover, during any attempt to fabricate much bigger BMG size through PBF-LB/M, a partial crystallisation occurred [183]. Therefore, to address the current challenges and satisfy the future requirement for the fabrication of biomedical BMG devices through PBF-LB/M techniques, there is a need for the future studies to focus more on: (i) improving the proven biomedical alloys GFA (ii) optimizing the PBF-LB/M process parameters for achieving larger BMGs without compromising the amorphous structure of the biomedical BMGs and (iii) explore on more biocompatible elements with high GFA.

5.5 Post-processing of PBF-LB/M processed BMG part

It is quite challenging to fabricate biomedical BMGs components through PBF-LB/M with high precision and satisfactory surface quality without compromising certain materials properties, product performance or manufacturing efficiency. Apart from highly rough surface produced during PBF-LB/M, most of the BMG parts contained some defects such as microcracks, undesigned porosities, unmelted powders and crystalline HAZ (Tables 3 to 5) [333]. This seriously affects the properties, quality and the performance of the final products. Several post-processing approaches such as (i) heat treatment, which reduce thermal stresses that accumulated during PBF-LB/M and enhance the microstructural defects; (ii) surface coating, which enhance tissues adhesion and block the release of toxic elements into the surrounding tissues; and (iii) grinding or polishing, which removes the partially melt particles after the PBF-LB/M of the BMG part and tailor the fabricated BMG surface roughness to match the human bone structure. Post-processing of PBF-LB/M processed BMG implant is expected

to play a vital role in upgrading the BMG implant quality, accuracy and performance in the host body [334, 335]. Moreover, surface modification was revealed to enhance the mechanical, physical and biological behaviours of the BMG implants without compromising its amorphous nature [336]. Therefore, exploring on proper techniques for the surface treatment of biomedical BMGs will play a significant role in the future research directions. The most critical challenge is selecting the best surface modification methods, which will not destroy the amorphous nature of the BMGs. On the other hand, employing PBF-LB/M techniques to modify or coat the surface of biomedical BMGs might be a good future research direction.

5.6 PBF-LB/M of BMG composite

Despite the extremely high hardness and strength of BMGs, they are characterised with a very low fracture toughness with no or very little plasticity. This is a serious challenge of all BMG systems, which might lead to BMG implant failure, especially when subjected to loading condition [236]. Although efforts have been devoted to enhancing the plasticity and the toughness of the BMGs by reinforcing in-situ second ductile crystalline phase through PBF-LB/M techniques to form BMG composites, the problems of cracks formation, porosities and incomplete powder melting still persist [289, 291, 337, 338]. Therefore, future studies that will focus on fabricating ductile BMGs composites with fully amorphous structure and maintaining the mechanical and biomedical behaviours of biomedical BMGs will be of great interest. Additionally, optimizing the ductility and the fracture toughness by controlling the second phase may enhance the processability of biomedical BMG composite through PBF-LB/M.

6. Summary and conclusion

The emergence of laser powder-bed fusion (PBF-LB/M) processes in fabricating bulk metallic glasses (BMGs), particularly for the fabrication of biomedical BMG components has recently witnessed an enormous acceptance. This may relate to its capability to fabricate record large, complex and customer-tailored BMG parts with properties comparable to those processed through conventional techniques. Figure 23 shows a research trend on the PBF-LB/M of Zr-, Fe- and Ti-based BMGs from 2012 to 2022. A sharp progressive rise in publications on PBF-LB/M of BMGs was noticed since the last 10 years with highest publications in 2022. This further confirmed the widespread acceptability of PBF-LB/M techniques for the fabrication of biomedical BMG parts. Among the biomedical BMG systems processed through PBF-LB/M, Zr-based is the most studied, which account for the 60 % of the recently published articles. The major focus of the current researches is on investigating the processability and fabrication of record-size BMG parts by varying PBF-LB/M process parameters like scan speed, laser power, scan spacing, layer thickness and scanning strategy. Laser energy, laser power and scanning strategy were found to have the strongest influence on the amorphous structure, pores and micro-cracks formation. Some researchers also studied the glass forming ability (GFA) of various alloy compositions and revealed that, even alloys with low GFA can be processed through PBF-LB/M.
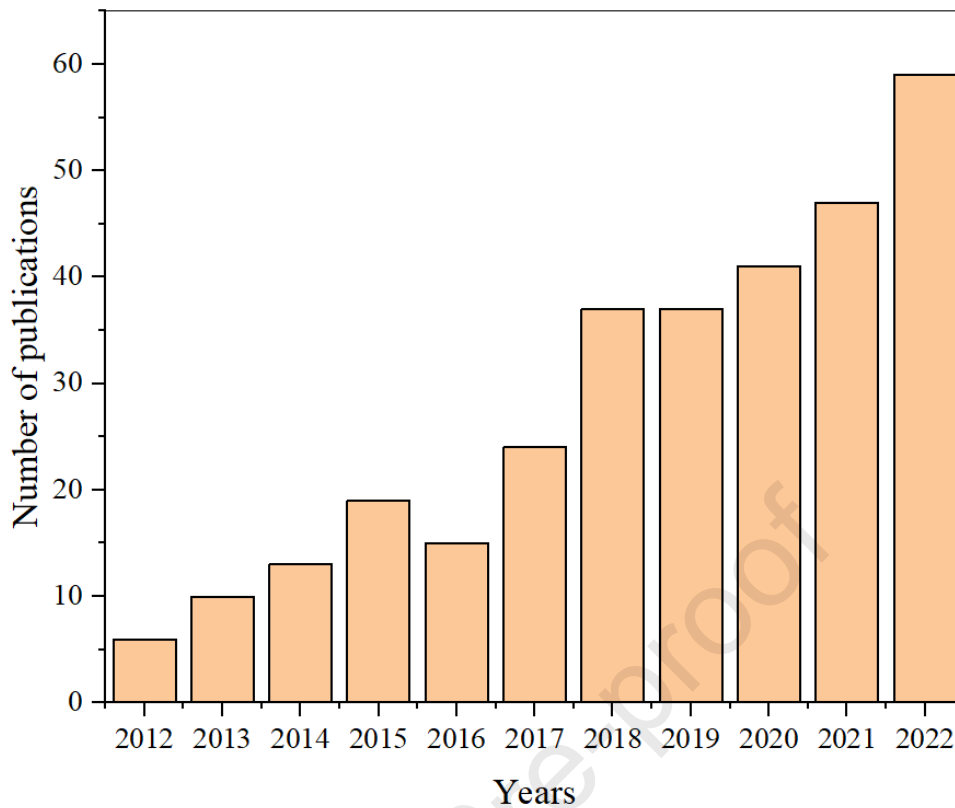
Figure 23: PBF-LB/M of BMGs, a statistical summary of published articles in the last 10 years based on Google Scholar database. The keywords used for the searching include laser, additive manufacturing, bulk metallic glass

Currently there are numerous challenges which need to be addressed before PBF-LB/M techniques accepted by the industries and production of commercial BMG implants. The major challenge is partial crystallisation, which degrades the inherent biomechanical and biomedical behaviours of BMGs. Other challenges are the formation of undesigned pores and microcracks, which are mostly observed in the final biomedical BMG components. Although, these challenges were improved by varying some PBF-LB/M process parameters, there still a long way to go and this improvement was achieved at the expense of other critical biomedical BMG requirements or properties. The PBF-LB/M process parameters optimisation, post-processing of the PBF-LB/M fabricated components and enhancing BMGs plasticity by developing novel BMGs composites, are proposed to be the best route for addressing the current limitations of PBF-LB/M techniques in fabricating BMGs. Despite these challenges, PBF-LB/M outweighed

the currently used conventional BMG fabrication techniques due to their capability to fabricate larger BMG geometries, technologically complex and customized BMG parts. The future research trends are expected to gain more attention towards overcoming these challenges and advancing the BMG size to an industrial and clinical grade biomaterial.

Acknowledgement

References

[1]   K. Prasad *et al.*, "Metallic biomaterials: Current challenges and opportunities," *Materials,* vol. 10, no. 8, p. 884, 2017.

[2]   P. Kittichokechai, K. Sirichatchai, C. Puncreobutr, B. Lohwongwatana, and P. Saonanon, "A Novel Patient-specific Titanium Mesh Implant Design for Reconstruction of Complex Orbital Fracture," *Plastic and Reconstructive Surgery–Global Open,* vol. 10, no. 1, p. e4081, 2022.

[3]   H. Kabir, K. Munir, C. Wen, and Y. Li, "Recent research and progress of biodegradable zinc alloys and composites for biomedical applications: biomechanical and biocorrosion perspectives," *Bioactive Materials,* vol. 6, no. 3, pp. 836-879, 2021.

[4]   R. Zan *et al.*, "Biodegradable magnesium implants: a potential scaffold for bone tumor patients," *Science China Materials,* vol. 64, no. 4, pp. 1007-1020, 2021.

[5]   K. Li, B. Li, P. Du, T. Xiang, X. Yang, and G. Xie, "Effect of powder size on strength and corrosion behavior of Mg66Zn30Ca4 bulk metallic glass," *Journal of Alloys and Compounds,* vol. 897, p. 163219, 2022.

[6]   K. Li *et al.*, "Mechanical properties and corrosion resistance of powder metallurgical Mg-Zn-Ca/Fe bulk metal glass composites for biomedical application," *Journal of Materials Science & Technology,* vol. 103, pp. 73-83, 2022.

[7]   K. Li, Z. Cai, P. Du, T. Xiang, X. Yang, and G. Xie, "Core-shell Mg66Zn30Ca4 bulk metallic glasses composites reinforced by Fe with high strength and controllable degradation," *Intermetallics,* vol. 138, p. 107334, 2021.

[8]   M. Razak, A. Rani, N. Saad, G. Littlefair, and A. Aliyu, "Controlling corrosion rate of Magnesium alloy using powder mixed electrical discharge machining," in *IOP Conference Series: Materials Science and Engineering*, 2018, vol. 344, no. 1: IOP Publishing, p. 012010.

[9]   M. A. H. A. Razak, A. M. Abdul-Rani, and A. A. A. Aliyu, "Innovative surface engineering technique for surface modification of Mg alloy for orthopedic application," in *Biomanufacturing*: Springer, 2019, pp. 225-240.

[10]   M. B. Nasab, M. R. Hassan, and B. B. Sahari, "Metallic biomaterials of knee and hip-a review," *Trends Biomater. Artif. Organs,* vol. 24, no. 1, pp. 69-82, 2010.

[11]   B. Vamsi Krishna, W. Xue, S. Bose, and A. Bandyopadhyay, "Engineered porous metals for implants," *Jom,* vol. 60, no. 5, pp. 45-48, 2008.

[12]   M. Niinomi, T. Narushima, and M. Nakai, "Advances in metallic biomaterials," *Niinomi, M., Narushima, T., Nakai, M., Eds,* 2015.

[13]   M. A. Hussein, A. S. Mohammed, and N. Al-Aqeeli, "Wear characteristics of metallic biomaterials: a review," *Materials,* vol. 8, no. 5, pp. 2749-2768, 2015.

[14]   R. M. Pilliar, "Metallic biomaterials," in *Biomedical materials*: Springer, 2021, pp. 1-47.

[15]   A. Bandyopadhyay, I. Mitra, S. B. Goodman, M. Kumar, and S. Bose, "Improving Biocompatibility for Next Generation of Metallic Implants," *Progress in Materials Science,* p. 101053, 2022.

[16]   J. Schroers, B. Lohwongwatana, W. L. Johnson, and A. Peker, "Precious bulk metallic glasses for jewelry applications," *Materials Science and Engineering: A,* vol. 449, pp. 235-238, 2007.

[17]   J. Schroers, B. Lohwongwatana, W. L. Johnson, and A. Peker, "Gold based bulk metallic glass," *Applied Physics Letters,* vol. 87, no. 6, p. 061912, 2005.

[18]   W. Klement, R. Willens, and P. Duwez, "Non-crystalline structure in solidified gold–silicon alloys," *Nature,* vol. 187, no. 4740, pp. 869-870, 1960.

[19]   P. Bordeenithikasem *et al.*, "Determination of critical cooling rates in metallic glass forming alloy libraries through laser spike annealing," *Scientific reports,* vol. 7, no. 1, pp. 1-9, 2017.

[20]   E. Axinte, A. Bofu, Y. Wang, A. M. Abdul-Rani, and A. A. A. Aliyu, "An overview on the conventional and nonconventional methods for manufacturing the metallic glasses," in *MATEC Web of Conferences*, 2017, vol. 112: EDP Sciences, p. 03003.

[21]   D. Xu, B. Lohwongwatana, G. Duan, W. L. Johnson, and C. Garland, "Bulk metallic glass formation in binary Cu-rich alloy series–Cu100− xZrx (x= 34, 36, 38.2, 40 at.%) and mechanical properties of bulk Cu64Zr36 glass," *Acta Materialia,* vol. 52, no. 9, pp. 2621-2624, 2004.

[22]   L. Tian *et al.*, "Approaching the ideal elastic limit of metallic glasses," *Nature communications,* vol. 3, no. 1, pp. 1-6, 2012.

[23]   C.-Y. Lin, M.-C. Lee, and T.-S. Chin, "Fe–Y–M–B (M= Nb or Ta) bulk metallic glasses with ultrahigh strength and good soft magnetic properties," *Journal of Physics D: Applied Physics,* vol. 40, no. 2, p. 310, 2007.

[24]   A. A. Tsarkov, A. Y. Churyumov, V. Y. Zadorozhnyy, and D. V. Louzguine-Luzgin, "High-strength and ductile (Ti–Ni)-(Cu–Zr) crystalline/amorphous composite materials with superelasticity and TRIP effect," *Journal of Alloys and Compounds,* vol. 658, pp. 402-407, 2016.

[25]   F.-F. Wu, K. C. Chan, S.-S. Jiang, S.-H. Chen, and G. Wang, "Bulk metallic glass composite with good tensile ductility, high strength and large elastic strain limit," *Scientific reports,* vol. 4, no. 1, pp. 1-6, 2014.

[26]   Z. Zhu, H. Zhang, D. Pan, W. Sun, and Z. Hu, "Fabrication of Binary Ni-Nb Bulk Metallic Glass With High Strength and Compressive Plasticity," *Advanced Engineering Materials,* vol. 8, no. 10, pp. 953-957, 2006.

[27]   J. Fornell *et al.*, "Enhanced mechanical properties and in vitro corrosion behavior of amorphous and devitrified Ti40Zr10Cu38Pd12 metallic glass," *Journal of the mechanical behavior of biomedical materials,* vol. 4, no. 8, pp. 1709-1717, 2011.

[28]   J. Si, X. Chen, Y. Cai, Y. Wu, T. Wang, and X. Hui, "Corrosion behavior of Cr-based bulk metallic glasses in hydrochloric acid solutions," *Corrosion Science,* vol. 107, pp. 123-132, 2016.

[29]   T. Gloriant, "Microhardness and abrasive wear resistance of metallic glasses and nanostructured composite materials," *Journal of non-crystalline solids,* vol. 316, no. 1, pp. 96-103, 2003.

[30]   D. C. Hofmann *et al.*, "Optimizing bulk metallic glasses for robust, highly wear-resistant gears," *Advanced Engineering Materials,* vol. 19, no. 1, p. 1600541, 2017.

[31]   C. A. Schuh, T. C. Hufnagel, and U. Ramamurty, "Mechanical behavior of amorphous alloys," *Acta Materialia,* vol. 55, no. 12, pp. 4067-4109, 2007.

[32]   S. Tantavisut, B. Lohwongwatana, A. Khamkongkaeo, A. Tanavalee, P. Tangpornprasert, and P. Ittiravivong, "The novel toxic free titanium-based amorphous alloy for biomedical application," *Journal of Materials Research and Technology,* vol. 7, no. 3, pp. 248-253, 2018.

[33]   S. Tantavisut, B. Lohwongwatana, A. Khamkongkaeo, A. Tanavalee, P. Tangpornprasert, and P. Ittiravivong, "In vitro biocompatibility of novel titanium-based amorphous alloy thin film in human osteoblast like cells," *Chulalongkorn Medical Journal,* vol. 63, no. 2, pp. 89-93, 2019.

[34]   P. Du, T. Xiang, Z. Cai, and G. Xie, "The influence of porous structure on the corrosion behavior and biocompatibility of bulk Ti-based metallic glass," *Journal of Alloys and Compounds,* vol. 906, p. 164326, 2022.

[35]   P. Du, T. Xiang, X. Yang, and G. Xie, "Enhanced mechanical and antibacterial properties of Cu-bearing Ti-based bulk metallic glass by controlling porous structure," *Journal of Alloys and Compounds,* vol. 904, p. 164005, 2022.

[36]   P. Du, K. Li, B. Zhu, T. Xiang, and G. Xie, "Development of non-toxic low-cost bioactive porous Ti–Fe–Si bulk metallic glass with bone-like mechanical properties for orthopedic implants," *Journal of Materials Research and Technology,* vol. 17, pp. 1319-1329, 2022.

[37]   J. Qiao *et al.*, "Structural heterogeneities and mechanical behavior of amorphous alloys," *Progress in Materials Science,* vol. 104, pp. 250-329, 2019.

[38]   W. H. Wang, "Dynamic relaxations and relaxation-property relationships in metallic glasses," *Progress in Materials Science,* vol. 106, p. 100561, 2019.

[39]   J. F. Löffler, "Bulk metallic glasses," *Intermetallics,* vol. 11, no. 6, pp. 529-540, 2003.

[40]   D. C. Hofmann *et al.*, "Designing metallic glass matrix composites with high toughness and tensile ductility," *Nature,* vol. 451, no. 7182, pp. 1085-1089, 2008.

[41]   Z. Wang *et al.*, "Microstructure and mechanical behavior of metallic glass fiber-reinforced Al alloy matrix composites," *Scientific reports,* vol. 6, no. 1, pp. 1-11, 2016.

[42]   J. P. Kelly *et al.*, "Designing in situ and ex situ bulk metallic glass composites via spark plasma sintering in the super cooled liquid state," *Materials & Design,* vol. 93, pp. 26-38, 2016.

[43]   W. Zhang *et al.*, "A novel high-strength Al-based nanocomposite reinforced with Ti-based metallic glass nanoparticles produced by powder metallurgy," *Materials Science and Engineering: A,* vol. 734, pp. 34-41, 2018.

[44]   J. Schroers, "Processing of bulk metallic glass," *Advanced materials,* vol. 22, no. 14, pp. 1566-1597, 2010.

[45]   P. Du, Z. Wu, K. Li, T. Xiang, and G. Xie, "Porous Ti-based bulk metallic glass orthopedic biomaterial with high strength and low Young's modulus produced by one step SPS," *Journal of Materials Research and Technology,* vol. 13, pp. 251-259, 2021.

[46]   P. Du, B. Li, J. Chen, K. Li, and G. Xie, "Novel Ti-based bulk metallic glass free of toxic and noble elements for bio-implant applications," *Journal of Alloys and Compounds,* vol. 934, p. 167996, 2023.

[47]   A. Monfared, H. Vali, and S. Faghihi, "Biocorrosion and biocompatibility of Zr–Cu–Fe–Al bulk metallic glasses," *Surface and interface analysis,* vol. 45, no. 11-12, pp. 1714-1720, 2013.

[48]   S. Guo, L. Liu, N. Li, and Y. Li, "Fe-based bulk metallic glass matrix composite with large plasticity," *Scripta Materialia,* vol. 62, no. 6, pp. 329-332, 2010.

[49]   A. A. A. Aliyu *et al.*, "A new toxic-free Ti40Zr10Co36Pd14 metallic glass with good biocompatibility and surface behaviour comparable to Ti-6Al-4V," *Materials & Design,* vol. 218, p. 110691, 2022.

[50]   K. Filipecka, P. Pawlik, and J. Filipecki, "The effect of annealing on magnetic properties, phase structure and evolution of free volumes in Pr-Fe-BW metallic glasses," *Journal of Alloys and Compounds,* vol. 694, pp. 228-234, 2017.

[51]   R. Budhani, T. Goel, and K. Chopra, "Melt-spinning technique for preparation of metallic glasses," *Bulletin of Materials Science,* vol. 4, no. 5, pp. 549-561, 1982.

[52]   Y. Liu *et al.*, "Combinatorial development of antibacterial Zr-Cu-Al-Ag thin film metallic glasses," *Scientific reports,* vol. 6, no. 1, pp. 1-8, 2016.

[53]   S. Ding *et al.*, "Combinatorial development of bulk metallic glasses," *Nature Materials,* vol. 13, no. 5, pp. 494-500, 2014.

[54]   P. Zeman, M. Zítek, Š. Zuzjaková, and R. Čerstvý, "Amorphous Zr-Cu thin-film alloys with metallic glass behavior," *Journal of Alloys and Compounds,* vol. 696, pp. 1298-1306, 2017.

[55]   C. J. Lin and F. Spaepen, "Fe-B glasses formed by picosecond pulsed laser quenching," *Applied Physics Letters,* vol. 41, no. 8, pp. 721-723, 1982.

[56]   S. Vitta, "The limits of glass formation by pulsed laser quenching in Nb-Ni alloys," *Scripta metallurgica et materialia,* vol. 25, pp. 2209-2214, 1991.

[57]   H. Davies and J. Hull, "Amorphous nickel produced by splat quenching," *Materials Science and Engineering,* vol. 23, no. 2-3, pp. 193-198, 1976.

[58]   A. Aliyu, A. Abdul-Rani, T. Ginta, C. Prakash, E. Axinte, and R. Fua-Nizan, "Fabrication of nanoporosities on metallic glass surface by hydroxyapatite mixed EDM for orthopedic application," in *Int Med Device Technol Conf*, 2017, pp. 168-171.

[59]   A. A. A. Aliyu *et al.*, "A review of additive mixed-electric discharge machining: current status and future perspectives for surface modification of biomedical implants," *Advances in Materials Science and Engineering,* vol. 2017, 2017.

[60]   A. A. A. Aliyu *et al.*, "Synthesis and characterization of bioceramic oxide coating on Zr-Ti-Cu-Ni-Be BMG by electro discharge process," in *International Scientific-Technical Conference MANUFACTURING*, 2019: Springer, pp. 518-531.

[61]   A. a. A. Aliyu *et al.*, "Hydroxyapatite electro discharge coating of Zr-based bulk metallic glass for potential orthopedic application," in *Key Engineering Materials*, 2019, vol. 796: Trans Tech Publ, pp. 123-128.

[62]   A. A. A. Aliyu *et al.*, "Electro-Discharge Machining of Zr67Cu11Ni10Ti9Be3: An Investigation on Hydroxyapatite Deposition and Surface Roughness," *Processes,* vol. 8, no. 6, p. 635, 2020.

[63]   A. M. Abdul-Rani *et al.*, "Characterization, adhesion strength and in-vitro cytotoxicity investigation of hydroxyapatite coating synthesized on Zr-based BMG by electro discharge process," *Surface and Coatings Technology,* vol. 370, pp. 213-226, 2019.

[64]   A. M. Abdul-Rani, A. A. A. Aliyu, S. Hastuty, T. L. Ginta, T. Rao, and S. Ali, "Enhancing surface quality of Zr-Cu-Ni-Ti-Be through hydroxyapatite mixed EDM for potential orthopedic application," in *AIP Conference Proceedings*, 2018, vol. 2035, no. 1: AIP Publishing LLC, p. 080010.

[65]   N. Li, W. Chen, and L. Liu, "Thermoplastic micro-forming of bulk metallic glasses: a review," *Jom,* vol. 68, no. 4, pp. 1246-1261, 2016.

[66]   B. Sarac and J. Eckert, "Thermoplasticity of metallic glasses: Processing and applications," *Progress in Materials Science,* p. 100941, 2022.

[67]   J. Shinjo and C. Panwisawas, "Digital materials design by thermal-fluid science for multi-metal additive manufacturing," *Acta Materialia,* vol. 210, p. 116825, 2021.

[68]   F. I. Azam, A. M. A. Rani, M. A. H. A. Razak, S. Ali, and A. a. A. Aliyu, "Additive Manufacturing Processes, Challenges and Applications: A Review," *Progress in Engineering Technology III,* pp. 93-111, 2021.

[69]   D. Decha-umphai *et al.*, "Effects of post-processing on microstructure and adhesion strength of TiO2 nanotubes on 3D-printed Ti-6Al-4V alloy," *Surface and Coatings Technology,* p. 127431, 2021.

[70]   T. Thomrungpiyathan, S. Luenam, B. Lohwongwatana, W. Sirichativapee, K. Nabudda, and C. Puncreobutr, "A custom-made distal humerus plate fabricated by selective laser melting," *Computer Methods in Biomechanics and Biomedical Engineering,* vol. 24, no. 6, pp. 585-596, 2021.

[71]   H.-t. Chunate *et al.*, "Titania Nanotube Architectures Synthesized on 3D-Printed Ti-6Al-4V Implant and Assessing Vancomycin Release Protocols," *Materials,* vol. 14, no. 21, p. 6576, 2021.

[72]   N. Sri-utenchai, N. Pengrung, K. SrikonKorn, C. Puncreobutr, B. Lohwongwatana, and P. Sa-ngasoongsong, "Using 3D Printing Technology for Corrective Biplanar Chevron Osteotomy with Customized Osteotomy Guide and Patient-Matched Monoblock Crosslink Plate in Treatment of Cubitus Varus Deformity: A Case Report and Technical Note," 2020.

[73]   N. Sri-Utenchai, N. Pengrung, K. Srikong, C. Puncreobutr, B. Lohwongwatana, and P. Sa-Ngasoongsong, "Three-dimensional printing technology for patient-matched instrument in treatment of cubitus varus deformity: A case report," *World Journal of Orthopedics,* vol. 12, no. 5, p. 338, 2021.

[74]   J. Hiemenz, "Additive manufacturing trends in aerospace," *White Paper, Stratasys, USA,* pp. 1-11, 2014.

[75]   V. Mohanavel, K. A. Ali, K. Ranganathan, J. A. Jeffrey, M. Ravikumar, and S. Rajkumar, "The roles and applications of additive manufacturing in the aerospace and automobile sector," *Materials Today: Proceedings,* vol. 47, pp. 405-409, 2021.

[76]   S. Wannarumon and E. L. Bohez, "Rapid prototyping and tooling technology in jewelry CAD," *Computer-Aided Design and Applications,* vol. 1, no. 1-4, pp. 569-575, 2004.

[77]   M. L. Griffith *et al.*, "Understanding the microstructure and properties of components fabricated by laser engineered net shaping (LENS)," *MRS Online Proceedings Library,* vol. 625, no. 1, pp. 9-20, 2000.

[78]   W. E. Frazier, "Metal additive manufacturing: a review," *Journal of Materials Engineering and performance,* vol. 23, no. 6, pp. 1917-1928, 2014.

[79]   W. Liu and J. DuPont, "Fabrication of functionally graded TiC/Ti composites by laser engineered net shaping," *Scripta materialia,* vol. 48, no. 9, pp. 1337-1342, 2003.

[80]   D. De Baere, W. Devesse, B. De Pauw, L. Smeesters, H. Thienpont, and P. Guillaume, "Spectroscopic monitoring and melt pool temperature estimation during the laser metal deposition process," *Journal of Laser Applications,* vol. 28, no. 2, p. 022303, 2016.

[81]   J. Song, Y. Li, Q. Deng, and D. Hu, "Research progress of laser cladding forming technology," *Jixie Gongcheng Xuebao(Chinese Journal of Mechanical Engineering),* vol. 46, no. 14, pp. 29-39, 2010.

[82]   N. Zhang, Y. Liu, W. Yang, and S.-J. Pang, "Formation and properties of a Zr-based amorphous coating by laser cladding," *Rare Metals,* pp. 1-6, 2018.

[83]   J. Shinjo and C. Panwisawas, "Chemical species mixing during direct energy deposition of bimetallic systems using titanium and dissimilar refractory metals for repair and biomedical applications," *Additive Manufacturing,* p. 102654, 2022.

[84]   G. Wang, H. Fan, Y. Huang, J. Shen, and Z. Chen, "A new TiCuHfSi bulk metallic glass with potential for biomedical applications," *Materials & Design (1980-2015),* vol. 54, pp. 251-255, 2014.

[85]   S. Pang, Y. Liu, H. Li, L. Sun, Y. Li, and T. Zhang, "New Ti-based Ti–Cu–Zr–Fe–Sn–Si–Ag bulk metallic glass for biomedical applications," *Journal of Alloys and Compounds,* vol. 625, pp. 323-327, 2015.

[86]   Y. Liu, S. Pang, H. Li, Q. Hu, B. Chen, and T. Zhang, "Formation and properties of Ti-based Ti–Zr–Cu–Fe–Sn–Si bulk metallic glasses with different (Ti+ Zr)/Cu ratios for biomedical application," *Intermetallics,* vol. 72, pp. 36-43, 2016.

[87]   C. Huang *et al.*, "Improvement of bio-corrosion resistance for Ti42Zr40Si15Ta3 metallic glasses in simulated body fluid by annealing within supercooled liquid region," *Materials Science and Engineering: C,* vol. 52, pp. 144-150, 2015.

[88]   C. Wang *et al.*, "Ti-Cu-Zr-Fe-Sn-Si-Ag-Pd Bulk Metallic Glasses with Potential for Biomedical Applications," *Metallurgical and Materials Transactions A,* vol. 52, no. 5, pp. 1559-1567, 2021.

[89]   C. Lin *et al.*, "Simulated body-fluid tests and electrochemical investigations on biocompatibility of metallic glasses," *Materials Science and Engineering: C,* vol. 32, no. 8, pp. 2578-2582, 2012.

[90]   Z. Liu *et al.*, "Novel low Cu content and Ni-free Zr-based bulk metallic glasses for biomedical applications," *Journal of non-crystalline solids,* vol. 363, pp. 1-5, 2013.

[91]   J. P. Best *et al.*, "Fracture and fatigue behaviour of a laser additive manufactured Zr-based bulk metallic glass," *Additive Manufacturing,* vol. 36, p. 101416, 2020.

[92]   K. Zhou, Y. Liu, S. Pang, and T. Zhang, "Formation and properties of centimeter-size Zr–Ti–Cu–Al–Y bulk metallic glasses as potential biomaterials," *Journal of Alloys and Compounds,* vol. 656, pp. 389-394, 2016.

[93]   T. Zhang *et al.*, "Investigations of new bulk metallic glass alloys fabricated using a high-pressure die-casting method based on industrial grade Zr raw material," *Journal of Alloys and Compounds,* vol. 792, pp. 851-859, 2019.

[94]   Y. Wang, H. Li, Y. Cheng, S. Wei, and Y. Zheng, "Corrosion performances of a Nickel-free Fe-based bulk metallic glass in simulated body fluids," *Electrochemistry Communications,* vol. 11, no. 11, pp. 2187-2190, 2009.

[95]   X. Gu, S. J. Poon, and G. J. Shiflet, "Mechanical properties of iron-based bulk metallic glasses," *Journal of Materials Research,* vol. 22, no. 2, pp. 344-351, 2007.

[96]   V. Ponnambalam, S. J. Poon, and G. J. Shiflet, "Fe-based bulk metallic glasses with diameter thickness larger than one centimeter," *Journal of Materials Research,* vol. 19, no. 5, pp. 1320-1323, 2004.

[97]   J. Shen, Q. Chen, J. Sun, H. Fan, and G. Wang, "Exceptionally high glass-forming ability of an FeCoCrMoCBY alloy," *Applied Physics Letters,* vol. 86, no. 15, p. 151907, 2005.

[98]   E. Park and D. Kim, "Formation of Ca–Mg–Zn bulk glassy alloy by casting into cone-shaped copper mold," *Journal of Materials Research,* vol. 19, no. 3, pp. 685-688, 2004.

[99]   K. Amiya and A. Inoue, "Formation and thermal stability of Ca-Mg-Ag-Cu bulk glassy alloys," *Materials Transactions,* vol. 43, no. 10, pp. 2578-2581, 2002.

[100]   R. Nowosielski, A. Bajorek, and R. Babilas, "Corrosion behavior of bioresorbable Ca-Mg-Zn bulk metallic glasses," *Journal of Non-Crystalline Solids,* vol. 447, pp. 126-133, 2016.

[101]   W. Jiao, K. Zhao, X. Xi, D. Zhao, M. Pan, and W. Wang, "Zinc-based bulk metallic glasses," *Journal of non-crystalline solids,* vol. 356, no. 35-36, pp. 1867-1870, 2010.

[102]   W. Jiao *et al.*, "Development of CaZn based glassy alloys as potential biodegradable bone graft substitute," *Journal of non-crystalline solids,* vol. 357, no. 22-23, pp. 3830-3840, 2011.

[103]   S. Bose, D. Ke, H. Sahasrabudhe, and A. Bandyopadhyay, "Additive manufacturing of biomaterials," *Progress in materials science,* vol. 93, pp. 45-111, 2018.

[104]   V. K. Balla and A. Bandyopadhyay, "Laser processing of Fe-based bulk amorphous alloy," *Surface and Coatings Technology,* vol. 205, no. 7, pp. 2661-2667, 2010.

[105]   B. Chen, T. Shi, and G. Liao, "Laser welding of Zr 41 Ti 14 Cu 12 Ni 10 Be 23 bulk metallic glass and zirconium metal," *Journal of Wuhan University of Technology-Mater. Sci. Ed.,* vol. 29, no. 4, pp. 786-788, 2014.

[106]   X. Li, M. Roberts, S. O'Keeffe, and T. Sercombe, "Selective laser melting of Zr-based bulk metallic glasses: Processing, microstructure and mechanical properties," *Materials & Design,* vol. 112, pp. 217-226, 2016.

[107]   G. Yang *et al.*, "Laser solid forming Zr-based bulk metallic glass," *Intermetallics,* vol. 22, pp. 110-115, 2012.

[108]   D. C. Hofmann, P. Bordeenithikasem, A. Pate, S. N. Roberts, and E. Vogli, "Developing processing parameters and characterizing microstructure and properties of an additively manufactured FeCrMoBC metallic glass forming alloy," *Advanced Engineering Materials,* vol. 20, no. 10, p. 1800433, 2018.

58

[109]   C. Zhang, W. Wang, Y.-C. Li, Y.-G. Yang, Y. Wu, and L. Liu, "3D printing of Fe-based bulk metallic glasses and composites with large dimensions and enhanced toughness by thermal spraying," *Journal of Materials Chemistry A,* vol. 6, no. 16, pp. 6800-6805, 2018.

[110]   C. Zhang, W. Wang, W. Xing, and L. Liu, "Understanding on toughening mechanism of bioinspired bulk metallic glassy composites by thermal spray additive manufacturing," *Scripta Materialia,* vol. 177, pp. 112-117, 2020.

[111]   V. V. Popov *et al.*, "Powder bed fusion additive manufacturing using critical raw materials: A review," *Materials,* vol. 14, no. 4, p. 909, 2021.

[112]   A. Hehr and M. Norfolk, "A comprehensive review of ultrasonic additive manufacturing," *Rapid Prototyping Journal,* 2019.

[113]   M. A. Gibson *et al.*, "3D printing metals like thermoplastics: Fused filament fabrication of metallic glasses," *Materials Today,* vol. 21, no. 7, pp. 697-702, 2018.

[114]   F. Audebert, R. Colaco, R. Vilar, and H. Sirkin, "Production of glassy metallic layers by laser surface treatment," *Scripta materialia,* vol. 48, no. 3, pp. 281-286, 2003.

[115]   R. Laquai, B. R. Müller, G. Kasperovich, J. Haubrich, G. Requena, and G. Bruno, "X-ray refraction distinguishes unprocessed powder from empty pores in selective laser melting Ti-6Al-4V," *Materials Research Letters,* vol. 6, no. 2, pp. 130-135, 2018.

[116]   Simon, "The future of 3D printing for medical applications," vol. 2022, ed, 2016.

[117]   Cranial implant created by additive manufacturing. *Scientistlive*. Available: https://www.scientistlive.com/content/cranial-implant-created-additive-manufacturing

[118]   H. R. Mendoza. "3D Printing Gives Cancer Patient New Ribs and Sternum in First-of-Its-Kind Surgery." https://3dprint.com/95371/3d-printed-ribs-and-sternum/ (accessed 2022).

[119]   "Additive manufacturing in medicine: Applications, restrictions and future scope." http://medineer.com/?p=69 (accessed 24/03/2022, 2022).

[120]   "China Food & Drug Administration Approves 3D Printed Hip Implants for Use." 3D print.com. https://3dprint.com/93098/china-fda-hip-implants-3d/ (accessed 29/03/2022).

[121]   "Additive Manufacturing Service." http://www.3epd.com/services/additive-manufacturing/ (accessed 31/03/2022).

[122]   S. A. Goehrke. "Impossible Objects Presents Model One 3D Printer." 3D print.com. https://3dprint.com/173381/impossible-objects-model-one/ (accessed.

[123]   E. E. Modic. (2017) Today's Medical Developments Available: https://www.todaysmedicaldevelopments.com/article/additive-manufacturing-medical-implants-lpw-exatech-92017/

[124]   Q. Li, D. Qin, Y. Lu, X. Zhu, and X. Lu, "Laser additive manufacturing of ductile Fe-based bulk metallic glass composite," *Journal of Materials Science & Technology,* vol. 121, pp. 148-153, 2022.

[125]   Y. Li, Y. Shen, M. C. Leu, and H.-L. Tsai, "Mechanical properties of Zr-based bulk metallic glass parts fabricated by laser-foil-printing additive manufacturing," *Materials Science and Engineering: A,* vol. 743, pp. 404-411, 2019.

[126]   H. Lashgari, M. Ferry, and S. Li, "Additive manufacturing of bulk metallic glasses: Fundamental principle, current/future developments and applications," *Journal of Materials Science & Technology,* 2022.

[127]   H. Schleifenbaum, W. Meiners, K. Wissenbach, and C. Hinke, "Individualized production by means of high power Selective Laser Melting," *CIRP Journal of manufacturing science and technology,* vol. 2, no. 3, pp. 161-169, 2010.

[128]   B. Vandenbroucke and J. P. Kruth, "Selective laser melting of biocompatible metals for rapid manufacturing of medical parts," *Rapid Prototyping Journal,* 2007.

[129]   J. Ding, S. Qu, L. Zhang, M. Y. Wang, and X. Song, "Geometric deviation and compensation for thin-walled shell lattice structures fabricated by high precision laser powder bed fusion," *Additive Manufacturing,* vol. 58, p. 103061, 2022.

[130]   S. Bremen, W. Meiners, and A. Diatlov, "Selective laser melting: A manufacturing technology for the future?," *Laser Technik Journal,* vol. 9, no. 2, pp. 33-38, 2012.

[131]   N. Wang *et al.*, "The effects of various processing parameters on the mechanical properties and biocompatibility of Fe-based bulk metallic glass processed by selective laser melting at the constant energy density," *Chinese Journal of Mechanical Engineering: Additive Manufacturing Frontiers,* p. 100038, 2022.

[132]   Q. Tao *et al.*, "Selective laser melting of CP-Ti to overcome the low cost and high performance trade-off," *Additive Manufacturing,* vol. 34, p. 101198, 2020.

[133]   C. Zhang, X.-m. Li, S.-Q. Liu, H. Liu, L.-J. Yu, and L. Liu, "3D printing of Zr-based bulk metallic glasses and components for potential biomedical applications," *Journal of Alloys and Compounds,* vol. 790, pp. 963-973, 2019.

[134]   P. Bordeenithikasem, Y. Shen, H.-L. Tsai, and D. C. Hofmann, "Enhanced mechanical properties of additively manufactured bulk metallic glasses produced through laser foil printing from continuous sheetmetal feedstock," *Additive Manufacturing,* vol. 19, pp. 95-103, 2018.

[135]   L. Deng, S. Wang, P. Wang, U. Kühn, and S. Pauly, "Selective laser melting of a Ti-based bulk metallic glass," *Materials Letters,* vol. 212, pp. 346-349, 2018.

[136]   X. Li, C. Kang, H. Huang, L. Zhang, and T. B. Sercombe, "Selective laser melting of an Al86Ni6Y4. 5Co2La1. 5 metallic glass: Processing, microstructure evolution and mechanical properties," *Materials Science and Engineering: A,* vol. 606, pp. 370-379, 2014.

[137]   N. Sohrabi *et al.*, "Additive manufacturing of a precious bulk metallic glass," *Applied Materials Today,* vol. 24, p. 101080, 2021.

[138]   P. Fischer, A. Blatter, V. Romano, and H. Weber, "Selective laser sintering of amorphous metal powder," *Applied Physics A,* vol. 80, no. 3, pp. 489-492, 2005.

[139]   C. Zhang, D. Ouyang, S. Pauly, and L. Liu, "3D printing of bulk metallic glasses," *Materials Science and Engineering: R: Reports,* vol. 145, p. 100625, 2021.

[140]   "Laser Additive Manufacturing." Mechatronic Vehicle System Laboratory. (accessed 20/05/2021, 2021).

[141]   C. Leinenbach, "Selective Laser Melting," ed: Swiss Federal Laboratories for Materials Science and Technology.

[142]   W.-H. Wang, C. Dong, and C. Shek, "Bulk metallic glasses," *Materials Science and Engineering: R: Reports,* vol. 44, no. 2-3, pp. 45-89, 2004.

[143]   J. J. Kruzic, "Bulk metallic glasses as structural materials: a review," *Advanced Engineering Materials,* vol. 18, no. 8, pp. 1308-1331, 2016.

[144]   X. Gu, S. J. Poon, G. J. Shiflet, and M. Widom, "Ductility improvement of amorphous steels: Roles of shear modulus and electronic structure," *Acta Materialia,* vol. 56, no. 1, pp. 88-94, 2008.

[145]   Z. Wu, P. Du, T. Xiang, K. Li, and G. Xie, "Ti-based bulk metallic glass implantable biomaterial with adjustable porosity produced by a novel pressure regulation method in spark plasma sintering," *Intermetallics,* vol. 131, p. 107105, 2021.

[146]   K. Imai, "In vivo investigation of Zr-based bulk metallic glasses sub-periosteally implanted on the bone surface," *Journal of Materials Science and Chemical Engineering,* vol. 4, no. 1, pp. 46-51, 2016.

[147]   N. Hua *et al.*, "A biocompatible Pd-based BMG with excellent corrosive-wear resistance for implant applications," *Intermetallics,* vol. 124, p. 106847, 2020.

[148]   C. Elias, J. Lima, R. Valiev, and M. Meyers, "Biomedical applications of titanium and its alloys," *Jom,* vol. 60, no. 3, pp. 46-49, 2008.

[149]   P. Lucas *et al.*, "Thermoelectric bulk glasses based on the Cu–As–Te–Se system," *Journal of Materials Chemistry A,* vol. 1, no. 31, pp. 8917-8925, 2013.

[150] N. Hua, L. Huang, W. Chen, W. He, and T. Zhang, "Biocompatible Ni-free Zr-based bulk metallic glasses with high-Zr-content: Compositional optimization for potential biomedical applications," *Materials Science and Engineering: C,* vol. 44, pp. 400-410, 2014.

[151] T. Li, P. Wong, S. Chang, P. Tsai, J. Jang, and J. Huang, "Biocompatibility study on Ni-free Ti-based and Zr-based bulk metallic glasses," *Materials Science and Engineering: C,* vol. 75, pp. 1-6, 2017.

[152] A. Esmaeili, S. A. Ghaffari, M. Nikkhah, F. M. Ghaini, F. Farzan, and S. Mohammadi, "Biocompatibility assessments of 316L stainless steel substrates coated by Fe-based bulk metallic glass through electro-spark deposition method," *Colloids and Surfaces B: Biointerfaces,* vol. 198, p. 111469, 2021.

[153] Y. C. Hu *et al.*, "A highly efficient and self-stabilizing metallic-glass catalyst for electrochemical hydrogen generation," *Advanced Materials,* vol. 28, no. 46, pp. 10293-10297, 2016.

[154] X. Wang, R. Li, Z. Li, R. Xiao, X.-B. Chen, and T. Zhang, "Design and preparation of nanoporous Ag–Cu alloys by dealloying Mg–(Ag, Cu)–Y metallic glasses for antibacterial applications," *Journal of Materials Chemistry B,* vol. 7, no. 26, pp. 4169-4176, 2019.

[155] W. Liu *et al.*, "A room-temperature magnetic semiconductor from a ferromagnetic metallic glass," *Nature communications,* vol. 7, no. 1, pp. 1-6, 2016.

[156] J. Chen and Z. Zhu, "The study on surface chemical modification of Fe71. 5Cu1Nb3Si13. 5B9V2 amorphous alloy ribbons and its piezomagnetic effect," *Journal of Magnetism and Magnetic Materials,* vol. 419, pp. 451-455, 2016.

[157] N. Chen *et al.*, "Transparent magnetic semiconductor with embedded metallic glass nano-granules," *Materials & Design,* vol. 132, pp. 208-214, 2017.

[158] H. Hermawan, D. Ramdan, and J. R. Djuansjah, "Metals for biomedical applications," *Biomedical engineering-from theory to applications,* vol. 1, pp. 411-430, 2011.

[159] Q. Chen and G. A. Thouas, "Metallic implant biomaterials," *Materials Science and Engineering: R: Reports,* vol. 87, pp. 1-57, 2015/01/01/ 2015, doi: https://doi.org/10.1016/j.mser.2014.10.001.

[160] L. Prashanth, K. K. Kattapagari, R. T. Chitturi, V. R. R. Baddam, and L. K. Prasad, "A review on role of essential trace elements in health and disease," *Journal of dr. ntr university of health sciences,* vol. 4, no. 2, p. 75, 2015.

[161] R. P. Verma, "Titanium based biomaterial for bone implants: A mini review," *Materials Today: Proceedings,* vol. 26, pp. 3148-3151, 2020/01/01/ 2020, doi: https://doi.org/10.1016/j.matpr.2020.02.649.

[162] A. Sharma, J. N. Waddell, K. C. Li, L. A Sharma, D. J. Prior, and W. J. Duncan, "Is titanium–zirconium alloy a better alternative to pure titanium for oral implant? Composition, mechanical properties, and microstructure analysis," *The Saudi Dental Journal,* 2020/08/29/ 2020, doi: https://doi.org/10.1016/j.sdentj.2020.08.009.

[163] Z. Li, Z. Huang, F. Sun, X. Li, and J. Ma, "Forming of metallic glasses: mechanisms and processes," *Materials Today Advances,* vol. 7, p. 100077, 2020.

[164] M. Chen, "A brief overview of bulk metallic glasses," *NPG Asia Materials,* vol. 3, no. 9, pp. 82-90, 2011.

[165] M. M. Khan, A. Nemati, Z. U. Rahman, U. H. Shah, H. Asgar, and W. Haider, "Recent advancements in bulk metallic glasses and their applications: a review," *Critical Reviews in Solid State and Materials Sciences,* vol. 43, no. 3, pp. 233-268, 2018.

[166] K. Hildal, N. Sekido, and J. Perepezko, "Critical cooling rate for Fe48Cr15Mo14Y2C15B6 bulk metallic glass formation," *Intermetallics,* vol. 14, no. 8-9, pp. 898-902, 2006.

[167] A. Takeuchi and A. Inoue, "Quantitative evaluation of critical cooling rate for metallic glasses," *Materials Science and Engineering: A,* vol. 304, pp. 446-451, 2001.

[168] D. Louzguine-Luzgin *et al.*, "Role of different factors in the glass-forming ability of binary alloys," *Journal of Materials Science,* vol. 50, no. 4, pp. 1783-1793, 2015.

[169] A. Inoue, "Stabilization of metallic supercooled liquid and bulk amorphous alloys," *Acta materialia,* vol. 48, no. 1, pp. 279-306, 2000.

[170] H. Chen, "Glassy metals," *Reports on Progress in Physics,* vol. 43, no. 4, p. 353, 1980.

[171] W. Zai, H. Man, Y. Su, G. Li, and J. Lian, "Impact of microalloying element Ga on the glass-forming ability (GFA), mechanical properties and corrosion behavior of Mg–Zn–Ca bulk metallic glass," *Materials Chemistry and Physics,* vol. 255, p. 123555, 2020.

[172] B. Li *et al.*, "Effects of Ag substitution for Fe on glass-forming ability, crystallization kinetics, and mechanical properties of Ni-free Zr–Cu–Al–Fe bulk metallic glasses," *Journal of Alloys and Compounds,* vol. 827, p. 154385, 2020.

[173] E. Park, H. Chang, D. Kim, T. Ohkubo, and K. Hono, "Effect of the substitution of Ag and Ni for Cu on the glass forming ability and plasticity of Cu60Zr30Ti10 alloy," *Scripta Materialia,* vol. 54, no. 9, pp. 1569-1573, 2006.

[174] N. Hua and W. Chen, "Enhancement of glass-forming ability and mechanical property of Zr-based Zr-Al-Ni bulk metallic glasses with addition of Pd," *Journal of Alloys and Compounds,* vol. 693, pp. 816-824, 2017.

[175] Z. Jin *et al.*, "Effect of Hf substitution Cu on glass-forming ability, mechanical properties and corrosion resistance of Ni-free Zr–Ti–Cu–Al bulk metallic glasses," *Journal of Alloys and Compounds,* vol. 806, pp. 668-675, 2019.

[176] K. Han, J. Qiang, Y. Wang, and P. Häussler, "Zr-Al-Co-Cu bulk metallic glasses for biomedical devices applications," *Journal of Alloys and Compounds,* vol. 729, pp. 144-149, 2017.

[177] A. Kuball *et al.*, "Development and characterization of titanium-based bulk metallic glasses," *Journal of Alloys and Compounds,* vol. 790, pp. 337-346, 2019.

[178] Y. Liu, S. Pang, W. Yang, N. Hua, P. K. Liaw, and T. Zhang, "Tribological behaviors of a Ni-free Ti-based bulk metallic glass in air and a simulated physiological environment," *Journal of Alloys and Compounds,* vol. 766, pp. 1030-1036, 2018.

[179] Y. Liu, G. Wang, H. Li, S. Pang, K. Chen, and T. Zhang, "TiCuZrFeSnSiSc bulk metallic glasses with good mechanical properties for biomedical applications," *Journal of Alloys and Compounds,* vol. 679, pp. 341-349, 2016.

[180] A. Inoue, C. Fan, J. Saida, and T. Zhang, "High-strength Zr-based bulk amorphous alloys containing nanocrystalline and nanoquasicrystalline particles," *Science and Technology of Advanced Materials,* vol. 1, no. 2, pp. 73-86, 2000.

[181] S. Aybar, "Solidification and crystallization behaviour of bulk glass forming alloys," 2007.

[182] J. R. Groza and J. F. Shackelford, *Materials processing handbook*. CRC press, 2007.

[183] J. Schroers, R. Busch, S. Bossuyt, and W. Johnson, "Crystallization behavior of the bulk metallic glass forming Zr41Ti14Cu12Ni10Be23 liquid," *Materials Science and Engineering: A,* vol. 304, pp. 287-291, 2001.

[184] R. Nowosielski, A. Januszka, and R. Babilas, "Thermal properties of Fe-based bulk metallic glasses," *Journal of Achievements in Materials and Manufacturing Engineering,* vol. 55, no. 2, pp. 349-354, 2012.

[185] M. Yamasaki, S. Kagao, and Y. Kawamura, "Thermal diffusivity and conductivity of Zr55Al10Ni5Cu30 bulk metallic glass," *Scripta Materialia,* vol. 53, no. 1, pp. 63-67, 2005.

[186] J. Zhou, W. Yang, C. Yuan, B. Sun, and B. Shen, "Ductile FeNi-based bulk metallic glasses with high strength and excellent soft magnetic properties," *Journal of Alloys and Compounds,* vol. 742, pp. 318-324, 2018.

[187] P. Gong, K. Yao, and Y. Shao, "Effects of Fe addition on glass-forming ability and mechanical properties of Ti–Zr–Be bulk metallic glass," *Journal of Alloys and Compounds,* vol. 536, pp. 26-29, 2012.

[188] C. Y. Yap *et al.*, "Review of selective laser melting: Materials and applications," *Applied physics reviews,* vol. 2, no. 4, p. 041101, 2015.

[189] I. O. f. Standardization, *Additive Manufacturing: General: Principles: Terminology*. ISO, 2015.

[190]   M. Holmberg *et al.*, "On surface losses in direct metal laser sintering printed millimeter and submillimeter waveguides," *Journal of Infrared, Millimeter, and Terahertz Waves,* vol. 39, no. 6, pp. 535-545, 2018.

[191]   A. Gebhardt, F.-M. Schmidt, J.-S. Hötter, W. Sokalla, and P. Sokalla, "Additive manufacturing by selective laser melting the realizer desktop machine and its application for the dental industry," *Physics Procedia,* vol. 5, pp. 543-549, 2010.

[192]   H. Yves-Christian, W. Jan, M. Wilhelm, W. Konrad, and P. Reinhart, "Net shaped high performance oxide ceramic parts by selective laser melting," *Physics Procedia,* vol. 5, pp. 587-594, 2010.

[193]   M. Kandis and T. Bergman, "A simulation-based correlation of the density and thermal conductivity of objects produced by laser sintering of polymer powders," *J. Manuf. Sci. Eng.,* vol. 122, no. 3, pp. 439-444, 2000.

[194]   D. D. Gu, W. Meiners, K. Wissenbach, and R. Poprawe, "Laser additive manufacturing of metallic components: materials, processes and mechanisms," *International materials reviews,* vol. 57, no. 3, pp. 133-164, 2012.

[195]   I. Jonas, W. Hembree, F. Yang, R. Busch, and A. Meyer, "Industrial grade versus scientific pure: Influence on melt properties," *Applied Physics Letters,* vol. 112, no. 17, p. 171902, 2018.

[196]   Z. Mahbooba *et al.*, "Additive manufacturing of an iron-based bulk metallic glass larger than the critical casting thickness," *Applied Materials Today,* vol. 11, pp. 264-269, 2018.

[197]   J. P. Best *et al.*, "Structural periodicity in laser additive manufactured Zr-based bulk metallic glass," *Applied Physics Letters,* vol. 115, no. 3, p. 031902, 2019.

[198]   P. Bordeenithikasem, M. Stolpe, A. Elsen, and D. C. Hofmann, "Glass forming ability, flexural strength, and wear properties of additively manufactured Zr-based bulk metallic glasses produced through laser powder bed fusion," *Additive Manufacturing,* vol. 21, pp. 312-317, 2018.

[199]   C. Suwanpreecha, E. Alabort, Y. T. Tang, C. Panwisawas, R. C. Reed, and A. Manonukul, "A novel low-modulus titanium alloy for biomedical applications: A comparison between selective laser melting and metal injection moulding," *Materials Science and Engineering: A,* vol. 812, p. 141081, 2021.

[200]   J. Hostetler *et al.*, "Selective Laser Sintering of Low Density, Low Coefficient of Thermal Expansion Silica Parts," in *Proceedings of Solid Freeform Fabrication Symposium. Austin, TX*, 2016, pp. 978-988.

[201]   M. Fateri and A. Gebhardt, "Selective laser melting of soda-lime glass powder," *International Journal of Applied Ceramic Technology,* vol. 12, no. 1, pp. 53-61, 2015.

[202]   Y. Shen, Y. Li, C. Chen, and H.-L. Tsai, "3D printing of large, complex metallic glass structures," *Materials & Design,* vol. 117, pp. 213-222, 2017.

[203]   J. Wegner *et al.*, "Influence of powder characteristics on the structural and the mechanical properties of additively manufactured Zr-based bulk metallic glass," *Materials & Design,* vol. 209, p. 109976, 2021.

[204]   M. Sharifian, F. Ghoveisi, and N. Firouzi Farrashbandi, "Inverse Bremsstrahlung absorption in under-dense plasma with Kappa distributed electrons," *AIP Advances,* vol. 7, no. 5, p. 055107, 2017.

[205]   Y. Li and D. Gu, "Parametric analysis of thermal behavior during selective laser melting additive manufacturing of aluminum alloy powder," *Materials & Design,* vol. 63, pp. 856-867, 2014.

[206]   S. Pauly, P. Wang, U. Kühn, and K. Kosiba, "Experimental determination of cooling rates in selectively laser-melted eutectic Al-33Cu," *Additive Manufacturing,* vol. 22, pp. 753-757, 2018.

[207]   D. Dai and D. Gu, "Influence of thermodynamics within molten pool on migration and distribution state of reinforcement during selective laser melting of AlN/AlSi10Mg

composites," *International Journal of Machine Tools and Manufacture,* vol. 100, pp. 14-24, 2016.

[208] S. Pauly *et al.*, "Processing metallic glasses by selective laser melting," *Materials Today,* vol. 16, no. 1-2, pp. 37-41, 2013.

[209] A. Inoue and A. Takeuchi, "Recent development and application products of bulk glassy alloys," *Acta Materialia,* vol. 59, no. 6, pp. 2243-2267, 2011.

[210] Z. Yang *et al.*, "Evolution of an industrial-grade Zr-based bulk metallic glass during multiple laser beam melting," *Journal of Non-Crystalline Solids,* vol. 589, p. 121649, 2022.

[211] V. Pacheco *et al.*, "Thermal stability and crystallization of a Zr-based metallic glass produced by suction casting and selective laser melting," *Journal of Alloys and Compounds,* vol. 825, p. 153995, 2020.

[212] Q. Lei, B. P. Ramakrishnan, S. Wang, Y. Wang, J. Mazumder, and A. Misra, "Structural refinement and nanomechanical response of laser remelted Al-Al2Cu lamellar eutectic," *Materials Science and Engineering: A,* vol. 706, pp. 115-125, 2017.

[213] Y. Liu, Z. Liu, Y. Jiang, G. Wang, Y. Yang, and L. Zhang, "Gradient in microstructure and mechanical property of selective laser melted AlSi10Mg," *Journal of Alloys and Compounds,* vol. 735, pp. 1414-1421, 2018.

[214] E. O. Olakanmi, R. Cochrane, and K. Dalgarno, "A review on selective laser sintering/melting (SLS/SLM) of aluminium alloy powders: Processing, microstructure, and properties," *Progress in Materials Science,* vol. 74, pp. 401-477, 2015.

[215] G. Tapia and A. Elwany, "A review on process monitoring and control in metal-based additive manufacturing," *Journal of Manufacturing Science and Engineering,* vol. 136, no. 6, 2014.

[216] S. K. Everton, M. Hirsch, P. Stravroulakis, R. K. Leach, and A. T. Clare, "Review of in-situ process monitoring and in-situ metrology for metal additive manufacturing," *Materials & Design,* vol. 95, pp. 431-445, 2016.

[217] D. Wu, Y. Wei, and J. Terpenny, "Predictive modelling of surface roughness in fused deposition modelling using data fusion," *International Journal of Production Research,* vol. 57, no. 12, pp. 3992-4006, 2019.

[218] Y. AbouelNour and N. Gupta, "In-situ monitoring of sub-surface and internal defects in additive manufacturing: A review," *Materials & Design,* p. 111063, 2022.

[219] A. M. Vest, D. R. St-Pierre, S. Rock, A. M. Maniatty, D. J. Lewis, and S. J. Hocker, "Thermocouple Temperature Measurements in Selective Laser Melting Additive Manufacturing," 2022.

[220] C. Kousiatza and D. Karalekas, "In-situ monitoring of strain and temperature distributions during fused deposition modeling process," *Materials & Design,* vol. 97, pp. 400-406, 2016.

[221] P. K. Rao, J. P. Liu, D. Roberson, Z. J. Kong, and C. Williams, "Online real-time quality monitoring in additive manufacturing processes using heterogeneous sensors," *Journal of Manufacturing Science and Engineering,* vol. 137, no. 6, 2015.

[222] P. K. Rao, J. Liu, D. Roberson, and Z. Kong, "Sensor-based online process fault detection in additive manufacturing," in *International Manufacturing Science and Engineering Conference*, 2015, vol. 56833: American Society of Mechanical Engineers, p. V002T04A010.

[223] C. K. P. Vallabh and X. Zhao, "Melt pool temperature measurement and monitoring during laser powder bed fusion based additive manufacturing via single-camera two-wavelength imaging pyrometry (STWIP)," *Journal of Manufacturing Processes,* vol. 79, pp. 486-500, 2022.

[224] A. Zinoviev, O. Zinovieva, V. Ploshikhin, V. Romanova, and R. Balokhonov, "Evolution of grain structure during laser additive manufacturing. Simulation by a cellular automata method," *Materials & Design,* vol. 106, pp. 321-329, 2016.

[225] Y. Li and D. Gu, "Thermal behavior during selective laser melting of commercially pure titanium powder: Numerical simulation and experimental study," *Additive Manufacturing,* vol. 1, pp. 99-109, 2014.

[226] M. Masoomi, S. Thompson, N. Shamsaei, A. Elwany, and L. Bian, "An experimental-numerical investigation of heat transfer during selective laser melting," in *26th International Solid Freeform Fabrication Symposium*, 2015, pp. 1-14.

[227] C. Tang, J. L. Tan, and C. H. Wong, "A numerical investigation on the physical mechanisms of single track defects in selective laser melting," *International Journal of Heat and Mass Transfer,* vol. 126, pp. 957-968, 2018.

[228] D. Ouyang, N. Li, W. Xing, J. Zhang, and L. Liu, "3D printing of crack-free high strength Zr-based bulk metallic glass composite by selective laser melting," *Intermetallics,* vol. 90, pp. 128-134, 2017.

[229] D. Ouyang, N. Li, and L. Liu, "Structural heterogeneity in 3D printed Zr-based bulk metallic glass by selective laser melting," *Journal of Alloys and Compounds,* vol. 740, pp. 603-609, 2018.

[230] K. Kosiba, D. Şopu, S. Scudino, L. Zhang, J. Bednarcik, and S. Pauly, "Modulating heterogeneity and plasticity in bulk metallic glasses: Role of interfaces on shear banding," *International Journal of Plasticity,* vol. 119, pp. 156-170, 2019.

[231] J. Lindwall, V. Pacheco, M. Sahlberg, A. Lundbäck, and L.-E. Lindgren, "Thermal simulation and phase modeling of bulk metallic glass in the powder bed fusion process," *Additive Manufacturing,* vol. 27, pp. 345-352, 2019.

[232] A. Nickel, D. Barnett, and F. Prinz, "Thermal stresses and deposition patterns in layered manufacturing," *Materials Science and Engineering: A,* vol. 317, no. 1-2, pp. 59-64, 2001.

[233] A. H. Nickel, "Analysis of thermal stresses in shape deposition manufacturing of metal parts," Citeseer, 1999.

[234] X. Nong, X. Zhou, and Y. Ren, "Fabrication and characterization of Fe-based metallic glasses by selective laser melting," *Optics & Laser Technology,* vol. 109, pp. 20-26, 2019.

[235] C. Panwisawas, Y. Gong, Y. T. Tang, R. C. Reed, and J. Shinjo, "Additive manufacturability of superalloys: Process-induced porosity, cooling rate and metal vapour," *Additive Manufacturing,* vol. 47, p. 102339, 2021.

[236] Y. Zou, Y. Wu, K. Li, C. Tan, Z. Qiu, and D. Zeng, "Selective laser melting of crack-free Fe-based bulk metallic glass via chessboard scanning strategy," *Materials Letters,* vol. 272, p. 127824, 2020.

[237] X. Li, C. Kang, H. Huang, and T. Sercombe, "The role of a low-energy–density re-scan in fabricating crack-free Al85Ni5Y6Co2Fe2 bulk metallic glass composites via selective laser melting," *Materials & Design,* vol. 63, pp. 407-411, 2014.

[238] J.-P. Kruth, L. Froyen, J. Van Vaerenbergh, P. Mercelis, M. Rombouts, and B. Lauwers, "Selective laser melting of iron-based powder," *Journal of materials processing technology,* vol. 149, no. 1-3, pp. 616-622, 2004.

[239] L. Parry, I. Ashcroft, and R. D. Wildman, "Understanding the effect of laser scan strategy on residual stress in selective laser melting through thermo-mechanical simulation," *Additive Manufacturing,* vol. 12, pp. 1-15, 2016.

[240] L. N. Carter *et al.*, "Process optimisation of selective laser melting using energy density model for nickel based superalloys," *Materials Science and Technology,* vol. 32, no. 7, pp. 657-661, 2016.

[241] H. Y. Jung *et al.*, "Fabrication of Fe-based bulk metallic glass by selective laser melting: A parameter study," *Materials & Design,* vol. 86, pp. 703-708, 2015.

[242] J. J. Marattukalam *et al.*, "Development of process parameters for selective laser melting of a Zr-based bulk metallic glass," *Additive Manufacturing,* vol. 33, p. 101124, 2020.

[243] L. Thijs, K. Kempen, J.-P. Kruth, and J. Van Humbeeck, "Fine-structured aluminium products with controllable texture by selective laser melting of pre-alloyed AlSi10Mg powder," *Acta Materialia,* vol. 61, no. 5, pp. 1809-1819, 2013.

[244]   J. Suryawanshi, K. Prashanth, S. Scudino, J. Eckert, O. Prakash, and U. Ramamurty, "Simultaneous enhancements of strength and toughness in an Al-12Si alloy synthesized using selective laser melting," *Acta Materialia,* vol. 115, pp. 285-294, 2016.

[245]   K. Prashanth, S. Scudino, T. Maity, J. Das, and J. Eckert, "Is the energy density a reliable parameter for materials synthesis by selective laser melting?," *Materials Research Letters,* vol. 5, no. 6, pp. 386-390, 2017.

[246]   B. V. Krishna, S. Bose, and A. Bandyopadhyay, "Low stiffness porous Ti structures for load-bearing implants," *Acta biomaterialia,* vol. 3, no. 6, pp. 997-1006, 2007.

[247]   A. Bandyopadhyay, F. Espana, V. K. Balla, S. Bose, Y. Ohgami, and N. M. Davies, "Influence of porosity on mechanical properties and in vivo response of Ti6Al4V implants," *Acta biomaterialia,* vol. 6, no. 4, pp. 1640-1648, 2010.

[248]   J.-Y. Buffiere, S. Savelli, P.-H. Jouneau, E. Maire, and R. Fougeres, "Experimental study of porosity and its relation to fatigue mechanisms of model Al–Si7–Mg0. 3 cast Al alloys," *Materials Science and Engineering: A,* vol. 316, no. 1-2, pp. 115-126, 2001.

[249]   J. Damon, S. Dietrich, F. Vollert, J. Gibmeier, and V. Schulze, "Process dependent porosity and the influence of shot peening on porosity morphology regarding selective laser melted AlSi10Mg parts," *Additive Manufacturing,* vol. 20, pp. 77-89, 2018.

[250]   I. Yadroitsev, A. Gusarov, I. Yadroitsava, and I. Smurov, "Single track formation in selective laser melting of metal powders," *Journal of Materials Processing Technology,* vol. 210, no. 12, pp. 1624-1631, 2010.

[251]   W. Xing, D. Ouyang, Z. Chen, and L. Liu, "Effect of energy density on defect evolution in 3D printed Zr-based metallic glasses by selective laser melting," *SCIENCE CHINA Physics, Mechanics & Astronomy,* vol. 63, no. 2, pp. 1-7, 2020.

[252]   L. Thijs, F. Verhaeghe, T. Craeghs, J. Van Humbeeck, and J.-P. Kruth, "A study of the microstructural evolution during selective laser melting of Ti–6Al–4V," *Acta materialia,* vol. 58, no. 9, pp. 3303-3312, 2010.

[253]   T. Gustmann *et al.*, "Influence of processing parameters on the fabrication of a Cu-Al-Ni-Mn shape-memory alloy by selective laser melting," *Additive Manufacturing,* vol. 11, pp. 23-31, 2016.

[254]   G. Flodberg, H. Pettersson, and L. Yang, "Pore analysis and mechanical performance of selective laser sintered objects," *Additive Manufacturing,* vol. 24, pp. 307-315, 2018.

[255]   J. Shi *et al.*, "3D pore structure characterization and hardness in a powder bed fusion-processed fully amorphous Zr-based bulk metallic glass," *Materials Characterization,* vol. 162, p. 110178, 2020.

[256]   C. Qiu, N. J. Adkins, and M. M. Attallah, "Microstructure and tensile properties of selectively laser-melted and of HIPed laser-melted Ti–6Al–4V," *Materials Science and Engineering: A,* vol. 578, pp. 230-239, 2013.

[257]   C. Qiu, C. Panwisawas, M. Ward, H. C. Basoalto, J. W. Brooks, and M. M. Attallah, "On the role of melt flow into the surface structure and porosity development during selective laser melting," *Acta Materialia,* vol. 96, pp. 72-79, 2015.

[258]   N. Read, W. Wang, K. Essa, and M. M. Attallah, "Selective laser melting of AlSi10Mg alloy: Process optimisation and mechanical properties development," *Materials & Design (1980-2015),* vol. 65, pp. 417-424, 2015.

[259]   M. Nematollahi *et al.*, "Additive manufacturing of Ni-rich NiTiHf20: manufacturability, composition, density, and transformation behavior," *Shape memory and superelasticity,* vol. 5, no. 1, pp. 113-124, 2019.

[260]   C. Liu, M. Zhang, and C. Chen, "Effect of laser processing parameters on porosity, microstructure and mechanical properties of porous Mg-Ca alloys produced by laser additive manufacturing," *Materials Science and Engineering: A,* vol. 703, pp. 359-371, 2017.

[261] S. V. Madge and A. L. Greer, "Laser additive manufacturing of metallic glasses: issues in vitrification and mechanical properties," *Oxford Open Materials Science,* vol. 1, no. 1, p. itab015, 2021.

[262] A. Strondl, O. Lyckfeldt, H. k. Brodin, and U. Ackelid, "Characterization and control of powder properties for additive manufacturing," *Jom,* vol. 67, no. 3, pp. 549-554, 2015.

[263] J. Buckley, "Additive Manufacturing in Orthopedics – Lattice Structures," vol. 2020, ed, 2020.

[264] R. Revanur, "3D Printing is grid locked in lattice structures," vol. 2022, ed, 2016.

[265] K. C. Wong, "3D-printed patient-specific applications in orthopedics," *Orthopedic research and reviews,* vol. 8, p. 57, 2016.

[266] (2019) How Topology Optimization Could Be the Key to Longer-Lasting Hip Implants. *Additive Manufacturine*. Available: https://www.additivemanufacturing.media/articles/how-topology-optimization-could-be-the-key-to-longer-lasting-hip-implants

[267] R. Yan *et al.*, "Electron beam melting in the fabrication of three-dimensional mesh titanium mandibular prosthesis scaffold," *Scientific Reports,* vol. 8, no. 1, pp. 1-10, 2018.

[268] F. Xie, Q. Chen, and J. Gao, "Brittle-ductile transition in laser 3D printing of Fe-based bulk metallic glass composites," *Metals,* vol. 9, no. 1, p. 78, 2019.

[269] D. Ouyang, P. Zhang, C. Zhang, and L. Liu, "Understanding of crystallization behaviors in laser 3D printing of bulk metallic glasses," *Applied Materials Today,* vol. 23, p. 100988, 2021.

[270] D. Ouyang, W. Xing, N. Li, Y. Li, and L. Liu, "Structural evolutions in 3D-printed Fe-based metallic glass fabricated by selective laser melting," *Additive Manufacturing,* vol. 23, pp. 246-252, 2018.

[271] Y. Lu *et al.*, "Study on the microstructure, mechanical property and residual stress of SLM Inconel-718 alloy manufactured by differing island scanning strategy," *Optics & Laser Technology,* vol. 75, pp. 197-206, 2015.

[272] F. Geiger, K. Kunze, and T. Etter, "Tailoring the texture of IN738LC processed by selective laser melting (SLM) by specific scanning strategies," *Materials Science and Engineering: A,* vol. 661, pp. 240-246, 2016.

[273] J. Vaithilingam, R. D. Goodridge, R. J. Hague, S. D. Christie, and S. Edmondson, "The effect of laser remelting on the surface chemistry of Ti6al4V components fabricated by selective laser melting," *Journal of Materials Processing Technology,* vol. 232, pp. 1-8, 2016.

[274] L. Pantělejev, D. Koutný, D. Paloušek, and J. Kaiser, "Mechanical and microstructural properties of 2618 al-alloy processed by SLM remelting strategy," in *Materials Science Forum*, 2017, vol. 891: Trans Tech Publ, pp. 343-349.

[275] Ł. Żrodowski *et al.*, "New approach to amorphization of alloys with low glass forming ability via selective laser melting," *Journal of Alloys and Compounds,* vol. 771, pp. 769-776, 2019.

[276] Y. G. Nam *et al.*, "Selective laser melting vitrification of amorphous soft magnetic alloys with help of double-scanning-induced compositional homogeneity," *Materials Letters,* vol. 261, p. 127068, 2020.

[277] D. Gu and Y. Shen, "Balling phenomena during direct laser sintering of multi-component Cu-based metal powder," *Journal of Alloys and Compounds,* vol. 432, no. 1-2, pp. 163-166, 2007.

[278] R. Li, Y. Shi, Z. Wang, L. Wang, J. Liu, and W. Jiang, "Densification behavior of gas and water atomized 316L stainless steel powder during selective laser melting," *Applied surface science,* vol. 256, no. 13, pp. 4350-4356, 2010.

[279] R. Li, J. Liu, Y. Shi, L. Wang, and W. Jiang, "Balling behavior of stainless steel and nickel powder during selective laser melting process," *The International Journal of Advanced Manufacturing Technology,* vol. 59, no. 9, pp. 1025-1035, 2012.

[280] N. Sohrabi, J. Jhabvala, and R. E. Logé, "Additive manufacturing of bulk metallic glasses—process, challenges and properties: a review," *Metals,* vol. 11, no. 8, p. 1279, 2021.

[281] M. Dambatta, S. Izman, B. Yahaya, J. Lim, and D. Kurniawan, "Mg-based bulk metallic glasses for biodegradable implant materials: A review on glass forming ability, mechanical

properties, and biocompatibility," *Journal of Non-Crystalline Solids,* vol. 426, pp. 110-115, 2015.

[282]   Y. Li, Y. Shen, C. Chen, M. C. Leu, and H.-L. Tsai, "Building metallic glass structures on crystalline metal substrates by laser-foil-printing additive manufacturing," *Journal of Materials Processing Technology,* vol. 248, pp. 249-261, 2017.

[283]   C. Yang, C. Zhang, W. Xing, and L. Liu, "3D printing of Zr-based bulk metallic glasses with complex geometries and enhanced catalytic properties," *Intermetallics,* vol. 94, pp. 22-28, 2018.

[284]   H. Xu, Y. Lu, Z. Liu, and G. Wang, "Laser 3D printing of Zr-based bulk metallic glass," *Journal of Manufacturing Processes,* vol. 39, pp. 102-105, 2019.

[285]   C. Fan, R. Ott, and T. Hufnagel, "Metallic glass matrix composite with precipitated ductile reinforcement," *Applied physics letters,* vol. 81, no. 6, pp. 1020-1022, 2002.

[286]   X. Li, M. Roberts, Y. Liu, C. Kang, H. Huang, and T. Sercombe, "Effect of substrate temperature on the interface bond between support and substrate during selective laser melting of Al–Ni–Y–Co–La metallic glass," *Materials & Design (1980-2015),* vol. 65, pp. 1-6, 2015.

[287]   X.-J. Shen, C. Zhang, Y.-G. Yang, and L. Liu, "On the microstructure, mechanical properties and wear resistance of an additively manufactured Ti64/metallic glass composite," *Additive Manufacturing,* vol. 25, pp. 499-510, 2019.

[288]   Z. Zhao, G. Yang, and K. Zhao, "3D Printing of Mg-Based Bulk Metallic Glasses with Proper Laser Power and Scanning Speed," *Metals,* vol. 12, no. 8, p. 1318, 2022.

[289]   N. Li, J. Zhang, W. Xing, D. Ouyang, and L. Liu, "3D printing of Fe-based bulk metallic glass composites with combined high strength and fracture toughness," *Materials & Design,* vol. 143, pp. 285-296, 2018.

[290]   S. Pauly, C. Schricker, S. Scudino, L. Deng, and U. Kühn, "Processing a glass-forming Zr-based alloy by selective laser melting," *Materials & Design,* vol. 135, pp. 133-141, 2017.

[291]   P. Zhang, D. Ouyang, and L. Liu, "Enhanced mechanical properties of 3D printed Zr-based BMG composite reinforced with Ta precipitates," *Journal of Alloys and Compounds,* vol. 803, pp. 476-483, 2019.

[292]   L. Deng *et al.*, "Mechanical performance and corrosion behaviour of Zr-based bulk metallic glass produced by selective laser melting," *Materials & Design,* vol. 189, p. 108532, 2020.

[293]   J. P. Best *et al.*, "Relating fracture toughness to micro-pillar compression response for a laser powder bed additive manufactured bulk metallic glass," *Materials Science and Engineering: A,* vol. 770, p. 138535, 2020.

[294]   H. Sun and K. Flores, "Microstructural analysis of a laser-processed Zr-based bulk metallic glass," *Metallurgical and Materials Transactions A,* vol. 41, no. 7, pp. 1752-1757, 2010.

[295]   K. Kosiba, L. Deng, and S. Scudino, "Viscous Flow of Supercooled Liquid in a Zr-Based Bulk Metallic Glass Synthesized by Additive Manufacturing," *Materials,* vol. 13, no. 17, p. 3803, 2020.

[296]   N. Sohrabi *et al.*, "Characterization, mechanical properties and dimensional accuracy of a Zr-based bulk metallic glass manufactured via laser powder-bed fusion," *Materials & Design,* vol. 199, p. 109400, 2021.

[297]   S. Li, Q. Wei, Q. Li, B. Jiang, Y. Chen, and Y. Sun, "Development of Fe-based bulk metallic glasses as potential biomaterials," *Materials Science and Engineering: C,* vol. 52, pp. 235-241, 2015.

[298]   M. Z. Ibrahim *et al.*, "Advancement of the artificial amorphous-crystalline structure of laser cladded FeCrMoCB on nickel-free stainless-steel for bone-implants," *Materials Chemistry and Physics,* vol. 227, pp. 358-367, 2019.

[299]   N. Hua *et al.*, "Corrosive wear behaviors and mechanisms of a biocompatible Fe-based bulk metallic glass," *Journal of Non-Crystalline Solids,* vol. 542, p. 120088, 2020.

[300]   L. Wang *et al.*, "Selective laser melting helps fabricate record-large bulk metallic glass: Experiments, simulation and demonstrative part," *Journal of Alloys and Compounds,* vol. 808, p. 151731, 2019.

[301]   W. Xing, D. Ouyang, N. Li, and L. Liu, "Insight into micro-cracking in 3D-printed Fe-based BMGs by selective laser melting," *Intermetallics,* vol. 103, pp. 101-106, 2018.

[302]   M. Geetha, A. K. Singh, R. Asokamani, and A. K. Gogia, "Ti based biomaterials, the ultimate choice for orthopaedic implants–a review," *Progress in materials science,* vol. 54, no. 3, pp. 397-425, 2009.

[303]   H. Li and Y. Zheng, "Recent advances in bulk metallic glasses for biomedical applications," *Acta biomaterialia,* vol. 36, pp. 1-20, 2016.

[304]   L. Zhang *et al.*, "Compressive plastic metallic glasses with exceptional glass forming ability in the Ti–Zr–Cu–Fe–Be alloy system," *Journal of Alloys and Compounds,* vol. 638, pp. 349-355, 2015.

[305]   N. Schnell, M. Schoeler, G. Witt, and S. Kleszczynski, "Experimental and numerical thermal analysis of the laser powder bed fusion process using in situ temperature measurements of geometric primitives," *Materials & Design,* vol. 209, p. 109946, 2021.

[306]   C. Panwisawas *et al.*, "Mesoscale modelling of selective laser melting: Thermal fluid dynamics and microstructural evolution," *Computational Materials Science,* vol. 126, pp. 479-490, 2017.

[307]   C. Panwisawas, C. Qiu, Y. Sovani, J. Brooks, M. Attallah, and H. Basoalto, "On the role of thermal fluid dynamics into the evolution of porosity during selective laser melting," *Scripta Materialia,* vol. 105, pp. 14-17, 2015.

[308]   F.-J. Gürtler, M. Karg, K.-H. Leitz, and M. Schmidt, "Simulation of laser beam melting of steel powders using the three-dimensional volume of fluid method," *Physics Procedia,* vol. 41, pp. 881-886, 2013.

[309]   S. Guo, M. Wang, Z. Zhao, Y. Zhang, X. Lin, and W. Huang, "Molecular dynamics simulation on the micro-structural evolution in heat-affected zone during the preparation of bulk metallic glasses with selective laser melting," *Journal of Alloys and Compounds,* vol. 697, pp. 443-449, 2017.

[310]   J. Lindwall, A. Malmelöv, A. Lundbäck, and L.-E. Lindgren, "Efficiency and accuracy in thermal simulation of powder bed fusion of bulk metallic glass," *Jom,* vol. 70, no. 8, pp. 1598-1603, 2018.

[311]   R. Conner, A. Rosakis, W. Johnson, and D. Owen, "FRACTURE TOUGHNESS DETERMINATION FOR A BE: RYLLIUM-BEARING BULK METALLIC GLASS," 1997.

[312]   M. Morrison *et al.*, "The electrochemical evaluation of a Zr-based bulk metallic glass in a phosphate-buffered saline electrolyte," *Journal of Biomedical Materials Research Part A: An Official Journal of The Society for Biomaterials, The Japanese Society for Biomaterials, and The Australian Society for Biomaterials and the Korean Society for Biomaterials,* vol. 74, no. 3, pp. 430-438, 2005.

[313]   A. A. A. Aliyu, A. M. Abdul-Rani, T. L. Ginta, T. Rao, N. Selvamurugan, and S. Roy, "Hydroxyapatite mixed-electro discharge formation of bioceramic Lakargiite (CaZrO3) on Zr–Cu–Ni–Ti–Be for orthopedic application," *Materials and Manufacturing Processes,* vol. 33, no. 16, pp. 1734-1744, 2018.

[314]   J. Horton and D. Parsell, "Biomedical potential of a zirconium-based bulk metallic glass," *Feb,* vol. 12, p. 6, 2003.

[315]   G. Welsch, R. Boyer, and E. Collings, *Materials properties handbook: titanium alloys*. ASM international, 1993.

[316]   M. Niinomi, "Mechanical properties of biomedical titanium alloys," *Materials Science and Engineering: A,* vol. 243, no. 1-2, pp. 231-236, 1998.

[317] N. Li, S. Wu, D. Ouyang, J. Zhang, and L. Liu, "Fe-based metallic glass reinforced FeCoCrNiMn high entropy alloy through selective laser melting," *Journal of Alloys and Compounds,* vol. 822, p. 153695, 2020.

[318] J. Xu, U. Ramamurty, and E. Ma, "The fracture toughness of bulk metallic glasses," *Jom,* vol. 62, no. 4, pp. 10-18, 2010.

[319] S. V. Madge, "Toughness of bulk metallic glasses," *Metals,* vol. 5, no. 3, pp. 1279-1305, 2015.

[320] P. Zhang, C. Zhang, and L. Liu, "Toughening 3D-printed Zr-based bulk metallic glass via synergistic defects engineering," *Materials Research Letters,* vol. 10, no. 6, pp. 377-384, 2022.

[321] N. Wang *et al.*, "Effects of Various Processing Parameters on Mechanical Properties and Biocompatibility of Fe-based Bulk Metallic Glass Processed via Selective Laser Melting at Constant Energy Density," *Chinese Journal of Mechanical Engineering: Additive Manufacturing Frontiers,* vol. 1, no. 3, p. 100038, 2022.

[322] L. Larsson, J. J. Marattukalam, E.-M. Paschalidou, B. r. Hjörvarsson, N. Ferraz, and C. Persson, "Biocompatibility of a Zr-Based Metallic Glass Enabled by Additive Manufacturing," *ACS Applied Bio Materials,* 2022.

[323] J.-H. Jang, H.-G. Kim, H.-J. Kim, and D.-G. Lee, "Crystallization and Hardness Change of the Ti-Based Bulk Metallic Glass Manufactured by a Laser Powder Bed Fusion Process," *Metals,* vol. 11, no. 7, p. 1049, 2021.

[324] Z. Yang, M. Markl, and C. Körner, "Predictive simulation of bulk metallic glass crystallization during laser powder bed fusion," *Additive Manufacturing,* vol. 59, p. 103121, 2022.

[325] Q. Jiang, H. Liu, J. Li, D. Yang, Y. Zhang, and W. Yang, "Atomic-level understanding of crystallization in the selective laser melting of Fe50Ni50 amorphous alloy," *Additive Manufacturing,* vol. 34, p. 101369, 2020.

[326] A. Greer, Y. Cheng, and E. Ma, "Shear bands in metallic glasses," *Materials Science and Engineering: R: Reports,* vol. 74, no. 4, pp. 71-132, 2013.

[327] J. Fu, H. Li, X. Song, and M. Fu, "Multi-scale defects in powder-based additively manufactured metals and alloys," *Journal of Materials Science & Technology,* 2022.

[328] J. Fu *et al.*, "Micro selective laser melting of NiTi shape memory alloy: Defects, microstructures and thermal/mechanical properties," *Optics & Laser Technology,* vol. 131, p. 106374, 2020.

[329] J. J. Williams and N. Chawla, "Fractography of a neck failure in a double-modular hip implant," *Case Studies in Engineering Failure Analysis,* vol. 2, no. 1, pp. 45-50, 2014.

[330] W. Xing, D. Ouyang, N. Li, and L. Liu, "Estimation of residual stress in selective laser melting of a zr-based amorphous alloy," *Materials,* vol. 11, no. 8, p. 1480, 2018.

[331] P. Mercelis and J. P. Kruth, "Residual stresses in selective laser sintering and selective laser melting," *Rapid prototyping journal,* 2006.

[332] H. Attar, M. Calin, L. Zhang, S. Scudino, and J. Eckert, "Manufacture by selective laser melting and mechanical behavior of commercially pure titanium," *Materials Science and Engineering: A,* vol. 593, pp. 170-177, 2014.

[333] B. LOHWONGWATANA, "Improvement of Titanium-based Bulk Metallic Glass Surface by Mechanical Process for Dental Implant Applications," 旭硝子財団助成研究成果報告 *Reports of research assisted by the Asahi Glass Foundation,* pp. 1-14, 2015.

[334] J. J. Ramsden *et al.*, "The design and manufacture of biomedical surfaces," *CIRP annals,* vol. 56, no. 2, pp. 687-711, 2007.

[335] J. Fu, S. Qu, J. Ding, X. Song, and M. Fu, "Effect of Heat Treatment on Microstructures and Mechanical Properties of SS316L by Micro Selective Laser Melting," in *International Manufacturing Science and Engineering Conference*, 2021, vol. 85062: American Society of Mechanical Engineers, p. V001T01A005.

[336]   X. Liu, P. K. Chu, and C. Ding, "Surface modification of titanium, titanium alloys, and related materials for biomedical applications," *Materials Science and Engineering: R: Reports,* vol. 47, no. 3-4, pp. 49-121, 2004.

[337]   Y. Zou, Z. Qiu, C. Tan, Y. Wu, K. Li, and D. Zeng, "Microstructure and mechanical properties of Fe-based bulk metallic glass composites fabricated by selective laser melting," *Journal of Non-Crystalline Solids,* vol. 538, p. 120046, 2020.

[338]   Y. Chen, C. Tang, and J.-Z. Jiang, "Bulk metallic glass composites containing B2 phase," *Progress in Materials Science,* vol. 121, p. 100799, 2021.

Declaration of interests

☒ The authors declare that they have no known competing financial interests or personal relationships that could have appeared to influence the work reported in this paper.

☐ The authors declare the following financial interests/personal relationships which may be considered as potential competing interests: